

NASA Contractor Report 4320

1N-02

7283

981

Visualization of Leading Edge Vortices on a Series of Flat Plate Delta Wings

Francis M. Payne, T. Terry Ng,
and Robert C. Nelson

GRANT NAG2-258
APRIL 1991

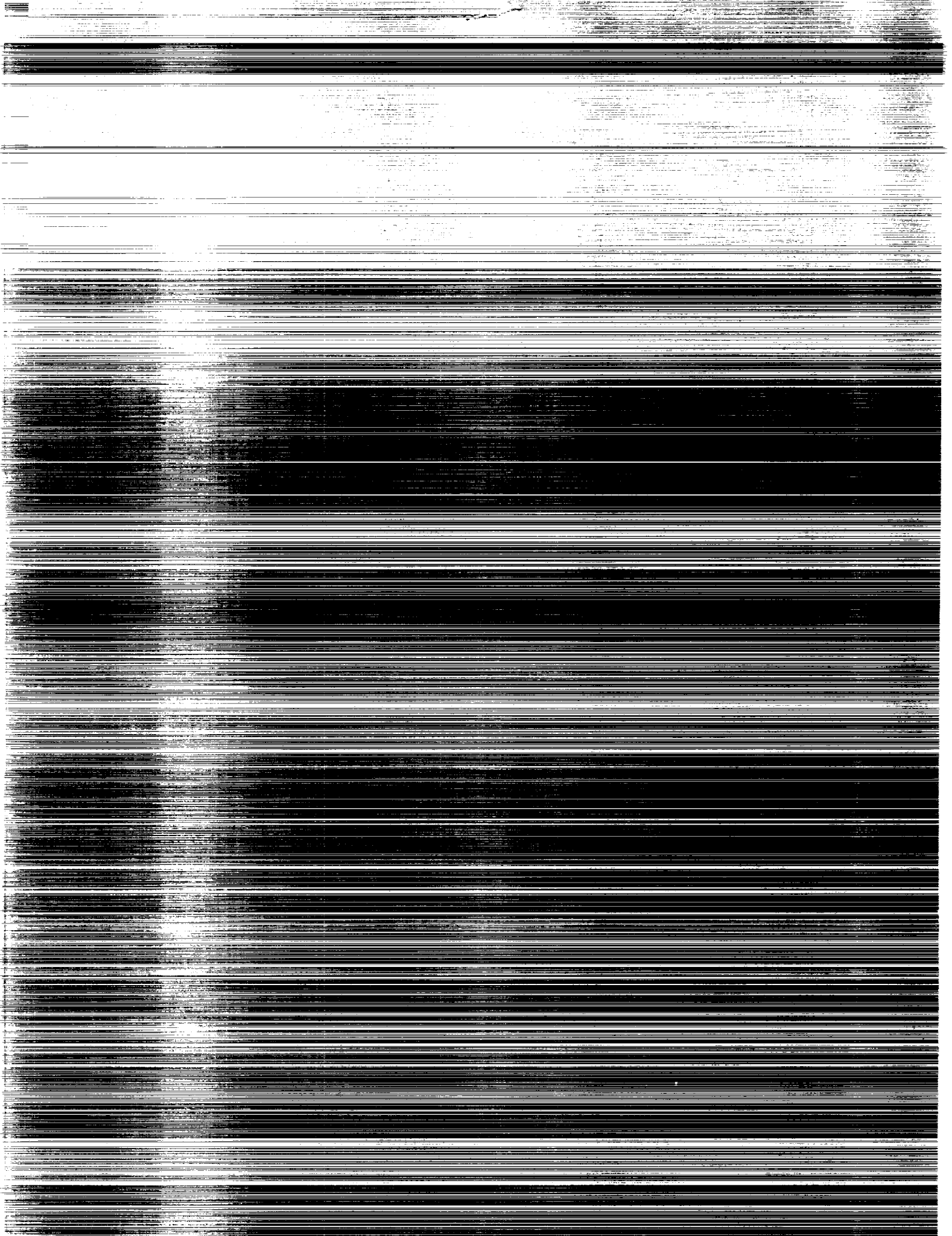
(NACA-CR-4320) VISUALIZATION OF LEADING
EDGE VORTICES ON A SERIES OF FLAT PLATE
DELTA WINGS (Notre Dame Univ.) 81 p

CSSL 01A

H1/02

Unclas

0007283



NASA Contractor Report 4320

Visualization of Leading Edge Vortices on a Series of Flat Plate Delta Wings

Francis M. Payne, T. Terry Ng,
and Robert C. Nelson
University of Notre Dame
Notre Dame, Indiana

Prepared for
Ames Research Center
under Grant NAG2-258



National Aeronautics and
Space Administration
Office of Management
Scientific and Technical
Information Division

1991



TABLE OF CONTENTS

Introduction----- 1
 1.1 Perspective ----- 1
 1.2 The Leading Edge Vortex----- 1
 1.3 Vortex Breakdown on Delta Wings----- 2
 1.4 Objectives----- 4
Experimental Apparatus----- 5
 2.1 Wind Tunnel----- 5
 2.2 Models----- 5
 2.3 Flow Visualization Equipment----- 6
Experimental Procedure and Results----- 8
 3.1 Smoke Flow Visualization----- 8
 3.2 Laser Light Sheet Technique----- 11
 3.3 Fluorescent Mini-Tufts----- 16
 3.4 High Speed Cinema----- 17
Conclusions----- 20
References ----- 21
Figures----- 24

LIST OF FIGURES

<u>Figure No.</u>		<u>Page No.</u>
1.1	Leading edge vortex flows on a delta wing	24
1.2	Types of breakdown on delta wings	25
2.1	Wind Tunnel	26
2.2	Sting and strut mounted models	27
2.3	Smoke generator	28
2.4	Smoke rake	29
3.1	Upstream smoke tube cross section	30
3.2	Schematic of laser light sheet technique	30
3.3	Laser sheet photographs showing secondary structure in shear layer. Sweep = 85° , Alpha = 20° , U = 3.0 m/s, x/c = 0.667 (top), x/c = 0.833 (bottom)	31
3.4	Laser sheet photograph showing outline of secondary structure in smoke. Sweep = 85° , Alpha = 35° , U = 3.0 m/s, x/c = 0.667	31
3.5	Diagram of flow with streamwise vortices	32
3.6	Lateral laser sheet cross section of bubble breakdown. Sweep = 85° , Alpha = 40° , U = 3.0 m/s	33
3.7	Longitudinal laser sheet cross section. Sweep = 80° , Alpha = 20° , U = 3.0 m/s	33
3.8	Longitudinal laser sheet cross sections of bubble type (top) and spiral type (bottom) breakdowns. Sweep = 85° , Alpha = 40° , U = 9.1 m/s	34
3.9	Position of vortex breakdown versus angle of attack	35
3.10	Symmetric bubble type breakdown. Longitudinal cross section. Enlargement from 16mm movie frame	36

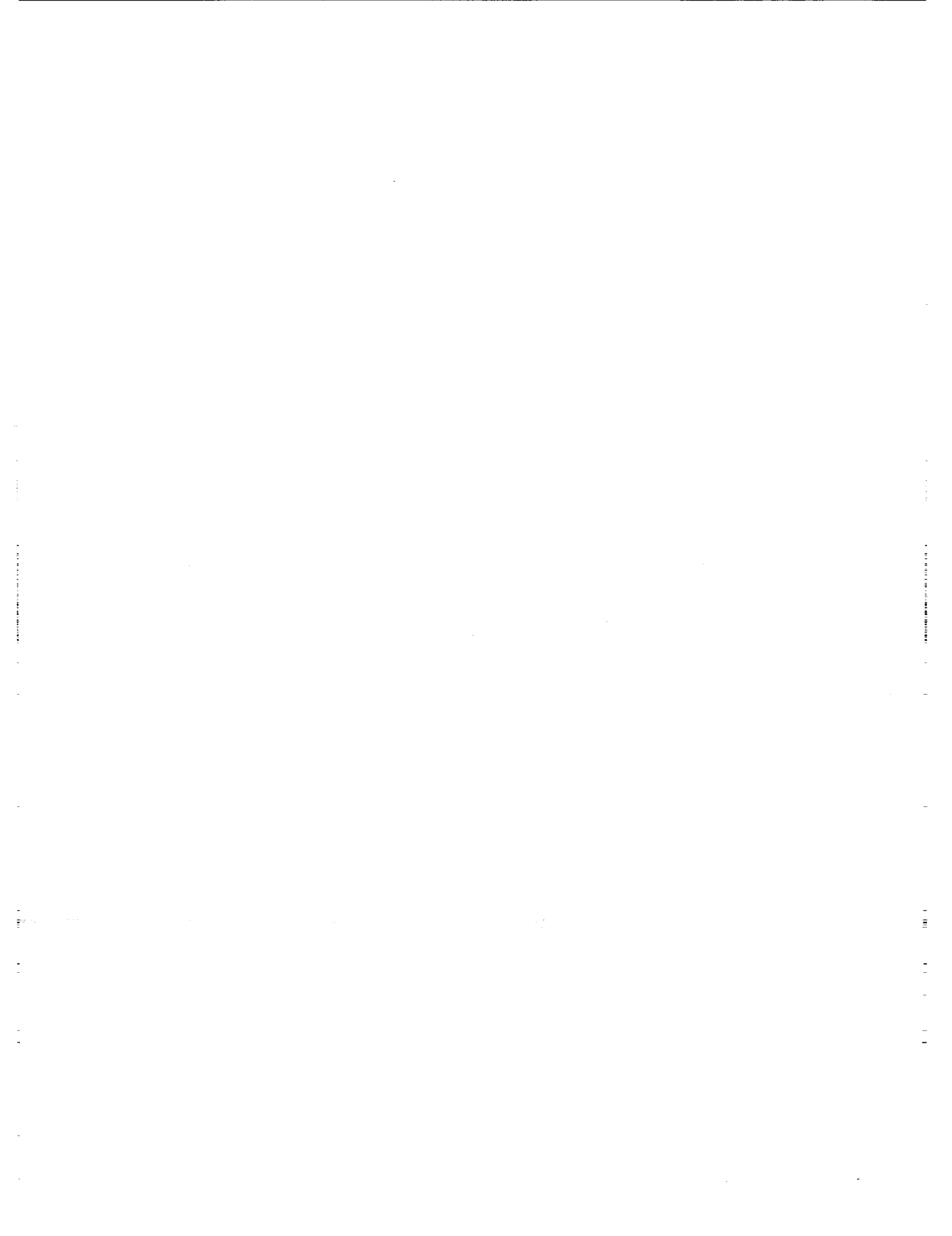
<u>Figure No.</u>		<u>Page No.</u>
3.11	Asymmetric bubble type breakdown. Longitudinal cross section. Enlargement from 16mm movie frame	36
3.12	Spiral type breakdown. Longitudinal cross section. Enlargement from 16mm movie frame	37
3.13	Bubble type breakdown. Lateral corss section. Enlargement from 16mm movie frame	38
3.14	Spiral type breakdown. Lateral cross section. Enlargement of 16mm movie frame	38
A1	Smoke flow visualization with flood lamp illumination. Sweep = 70° , Alpha = 10° , U = 3.0 m/s	39
A2	Smoke flow visualization with flood lamp illumination. Sweep = 70° , Alpha = 20° , U = 3.0 m/s	39
A3	Smoke flow visualization with flood lamp illumination. Sweep = 70° , Alpha = 30° , U = 3.0 m/s	40
A4	Smoke flow visualization with flood lamp illumination. Sweep = 70° , Alpha = 40° , U = 3.0 m/s	40
A5	Smoke flow visualization with flood lamp illumination Sweep = 75° , Alpha = 10° , U = 3.0 ft/s	41
A6	Smoke flow visualization with flood lamp illumination. Sweep = 75° , Alpha = 20° , U = 3.0 m/s	41
A7	Smoke flow visualization with flood lamp illumination. Sweep = 75° , Alpha = 30° , U = 3.0 m/s	42

<u>Figure No.</u>		<u>Page No.</u>
A8	Smoke flow visualization with flood lamp illumination. Sweep = 75°, Alpha = 40°, U = 3.0 m/s	42
A9	Smoke flow visualization with flood lamp illumination. Sweep = 80°, Alpha = 10°, U = 3.0 m/s	43
A10	Smoke flow visualization with flood lamp illumination. Sweep = 80°, Alpha = 20°, U = 3.0 m/s	43
A11	Smoke flow visualization with flood lamp illumination. Sweep = 80°, Alpha = 30°, U = 3.0 m/s	44
A12	Smoke flow visualization with flood lamp illumination. Sweep = 80°, Alpha = 40°, U = 3.0 m/s	44
A13	Smoke flow visualization with flood lamp illumination. Sweep = 85°, Alpha = 10°, U = 3.0 m/s	45
A14	Smoke flow visualization with flood lamp illumination. Sweep = 85°, Alpha = 20°, U = 3.0 m/s	45
A15	Smoke flow visualization with flood lamp illumination. Sweep = 85°, Alpha = 30°, U = 3.0 m/s	46
A16	Smoke flow visualization with flood lamp illumination. Sweep = 85°, Alpha = 40°, U = 3.0 m/s	46
A17	Lateral laser sheet cross sections. Sweep = 70°, Alpha = 10°, U = 3.0 m/s	47
A18	Lateral laser sheet cross sections. Sweep = 70°, Alpha = 20°, U = 3.0 m/s	47

<u>Figure No.</u>		<u>Page No.</u>
A19	Lateral laser sheet cross sections. Sweep = 70°, Alpha = 30°, U = 3.0 m/s	48
A20	Lateral laser sheet cross sections. Sweep = 70°, Alpha = 40°, U = 3.0 m/s	48
A21	Lateral laser sheet cross sections. Sweep = 75°, Alpha = 10°, U = 3.0 m/s	49
A22	Lateral laser sheet cross sections. Sweep = 75°, Alpha = 20°, U = 3.0 m/s	49
A23	Lateral laser sheet cross sections. Sweep = 75°, Alpha = 30°, U = 3.0 m/s	50
A24	Lateral laser sheet cross sections. Sweep = 75°, Alpha = 40°, U = 3.0 m/s	50
A25	Lateral laser sheet cross sections. Sweep = 80°, Alpha = 10°, U = 3.0 m/s	51
A26	Lateral laser sheet cross sections. Sweep = 80°, Alpha = 20°, U = 3.0 m/s	51
A27	Lateral laser sheet cross sections. Sweep = 80°, Alpha = 30°, U = 3.0 m/s	52
A28	Lateral laser sheet cross sections. Sweep = 80°, Alpha = 40°, U = 3.0 m/s	52
A29	Lateral laser sheet cross sections. Sweep = 85°, Alpha = 10°, U = 3.0 m/s	53
A30	Lateral laser sheet cross sections. Sweep = 85°, Alpha = 20°, U = 3.0 m/s	53
A31	Lateral laser sheet cross sections. Sweep = 85°, Alpha = 30°, U = 3.0 m/s	54
A32	Lateral laser sheet cross sections. Sweep = 85°, Alpha = 40°, U = 3.0 m/s	54
A33	Longitudinal laser sheet cross sections. Sweep = 70°, Alpha = 10°, U = 3.0 m/s	55

<u>Figure No.</u>		<u>Page No.</u>
A34	Longitudinal laser sheet cross sections. Sweep = 70°, Alpha = 20°, U = 3.0 m/s	55
A35	Longitudinal laser sheet cross sections. Sweep = 70°, Alpha = 30°, U = 3.0 m/s	56
A36	Longitudinal laser sheet cross sections. Sweep = 70°, Alpha = 40°, U = 3.0 m/s	56
A37	Longitudinal laser sheet cross sections. Sweep = 75°, Alpha = 10°, U = 3.0 m/s	57
A38	Longitudinal laser sheet cross sections. Sweep = 75°, Alpha = 20°, U = 3.0 m/s	57
A39	Longitudinal laser sheet cross sections. Sweep = 75°, Alpha = 30°, U = 3.0 m/s	58
A40	Longitudinal laser sheet cross sections. Sweep = 75°, Alpha = 40°, U = 3.0 m/s	58
A41	Longitudinal laser sheet cross sections. Sweep = 80°, Alpha = 10°, U = 3.0 m/s	59
A42	Longitudinal laser sheet cross sections. Sweep = 80°, Alpha = 20°, U = 3.0 m/s	59
A43	Longitudinal laser sheet cross sections. Sweep = 80°, Alpha = 30°, U = 3.0 m/s	60
A44	Longitudinal laser sheet cross sections. Sweep = 80°, Alpha = 40°, U = 3.0 m/s	60
A45	Longitudinal laser sheet cross sections. Sweep = 85°, Alpha = 10°, U = 3.0 m/s	61
A46	Longitudinal laser sheet cross sections. Sweep = 85°, Alpha = 20°, U = 3.0 m/s	61
A47	Longitudinal laser sheet cross sections. Sweep = 85°, Alpha = 30°, U = 3.0 m/s	62
A48	Longitudinal laser sheet cross sections. Sweep = 85°, Alpha = 40°, U = 3.0 m/s	62

<u>Figure No.</u>		<u>Page No.</u>
A49	Fluorescent mini-tufts. Sweep = 70°, Alpha = 10°, U = 15.2 m/s	63
A50	Fluorescent mini-tufts. Sweep = 70°, Alpha = 20°, U = 15.2 m/s	63
A51	Fluorescent mini-tufts. Sweep = 70°, Alpha = 30°, U = 15.2 m/s	64
A52	Fluorescent mini-tufts. Sweep = 70°, Alpha = 40°, U = 15.2 m/s	64
A53	Fluorescent mini-tufts. Sweep = 75°, Alpha = 10°, U = 15.2 m/s	65
A54	Fluorescent mini-tufts. Sweep = 75°, Alpha = 20°, U = 15.2 m/s	65
A55	Fluorescent mini-tufts. Sweep = 75°, Alpha = 30°, U = 15.2 m/s	66
A56	Fluorescent mini-tufts. Sweep = 75°, Alpha = 40°, U = 15.2 m/s	66
A57	Fluorescent mini-tufts. Sweep = 80°, Alpha = 10°, U = 15.2 m/s	67
A58	Fluorescent mini-tufts. Sweep = 80°, Alpha = 20°, U = 15.2 m/s	67
A59	Fluorescent mini-tufts. Sweep = 80°, Alpha = 30°, U = 15.2 m/s	68
A60	Fluorescent mini-tufts. Sweep = 80°, Alpha = 40°, U = 15.2 m/s	68
A61	Fluorescent mini-tufts. Sweep = 85°, Alpha = 10°, U = 15.2 m/s	69
A62	Fluorescent mini-tufts. Sweep = 85°, Alpha = 20°, U = 15.2 m/s	69
A63	Fluorescent mini-tufts. Sweep = 85°, Alpha = 30°, U = 15.2 m/s	70
A64	Fluorescent mini-tufts. Sweep = 85°, Alpha = 40°, U = 15.2 m/s	70

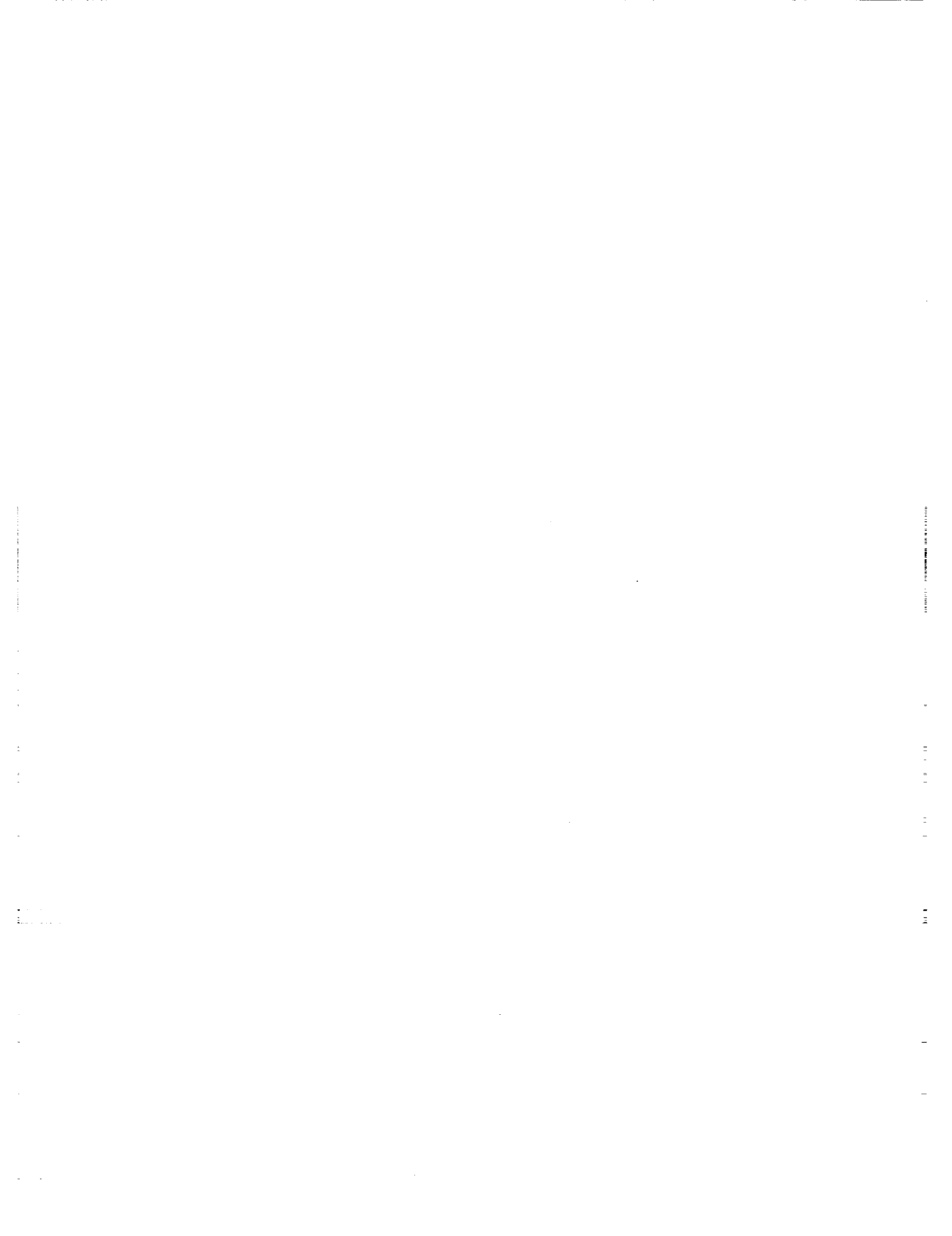


Acknowledgments

This research was supported by NASA Ames Research Center, Moffett Field, CA under grant number NAG2-258. The author wishes to thank Lewis B. Schiff, David Peake, Gary Erickson and Larry Erickson who served as technical monitors at various times during the course of this study.

~~24~~ X INTENTIONALLY BLANK

PRECEDING PAGE BLANK NOT FILMED



INTRODUCTION

1.1 Perspective

Leading edge vortex flows have been under study since the late 1950's when research and design work on delta wing aircraft was initiated. Interest in the phenomenon has intensified in recent years as concepts for highly maneuverable aircraft have been developed. At low speeds and moderate angles of attack the delta wing provides high lift by virtue of the strong vortices which emanate from the sharp leading edges. At supersonic speeds and low angles of attack the high sweep results in favorable drag characteristics. Thus the delta wing combines the advantages of efficient supersonic cruise with high g subsonic maneuver capability.

The aerodynamic characteristics of delta wings have been extensively studied in water tunnels, wind tunnels, and in flight. Leading edge vortex flows have been theoretically modeled and numerically simulated. However, in spite of this effort, many aspects of this type of flow are still not well understood.

This investigation uses smoke flow visualization and the laser light sheet technique in low speed wind tunnel tests to examine the structure of leading edge vortex flows on 70° , 75° , 80° , and 85° delta wings at angles of attack up to 40 degrees. The phenomenon of vortex breakdown is studied in detail to provide information for the analysis of breakdown theories and for comparison with computational results.

1.2 The Leading Edge Vortex

The flow structure on a delta wing at moderate to high angles of attack is extremely complex as shown in Figure 1.1. A pair of leading edge vortices will form on wings with sweep angles greater than about 45 degrees. The approaching flow initially attaches on the lower surface then turns outward and approaches the leading edge. Unable to negotiate the sharp turn, the flow separates and forms a shear layer or vortex sheet. A spanwise pressure gradient on the upper surface causes the shear layer to move inward and roll

up to form a concentrated vortex. Flow moving over the vortex is swept downward and reattaches on the surface of the wing before moving outward underneath the primary vortex towards the leading edge. Outboard of the vortex the surface boundary layer encounters an adverse pressure gradient which causes it to separate and form a smaller counter rotating secondary vortex.

The main effect of the secondary vortex is a displacement of the primary vortex upwards and inwards. This effect is greater if the upper surface boundary layer is laminar because flow separation occurs earlier and the secondary vortex is larger. Outboard of the secondary vortex the flow reattaches and approaches the leading edge. At the leading edge the flow again separates and joins the flow from the lower surface in the shear layer.

Flow passing over a delta wing is accelerated by the primary vortices which results in an increase of lift over what would be expected in the absence of the vortices. This additional lift is usually referred to as non-linear or vortex lift. It must be noted however, that the loss of leading edge suction due to flow separation also results in increased drag.

Along a ray from the apex to the trailing edge the static pressure falls rapidly near the apex then gradually rises over most of the wing until the trailing edge is approached where the pressure quickly recovers to near the freestream value.

The flow in the core of the vortex resembles a rotating jet. Axial velocities can reach more than three times the freestream value. A qualitative explanation for the high axial velocity along the core axis can be provided in terms of the spiral sheet model of the vortex.¹ The inclination of the spiraling vortex lines to the vortex axis is such as to make them all induce a downstream component of velocity along the axis.

1.3 Vortex Breakdown on Delta Wings

As the angle of attack of a delta wing is increased a leading edge vortex will grow in strength. The axial velocity in the core of the vortex can exceed three times the freestream value. At some

point along the vortex however a sudden transformation takes place causing the core flow to stagnate and the vortex to breakdown into large scale turbulence.

Peckham and Atkinson (1957)² were the first to observe vortex breakdown on a delta wing. Both Peckham (1958)³ and Elle (1958)⁴ showed that the position along the vortex at which breakdown occurs depends primarily on a combination of sweep and angle of attack. For highly swept wings at low angles of attack the breakdown occurs in the vortex downstream of the trailing edge, but with an increase of angle of attack or a decrease of sweep the breakdown moves upstream to a position above the surface of the wing. Breakdown results in the loss of lift on a wing and a change in pitching moment. The stability characteristics of an aircraft can also be adversely affected due to interaction of the breakdown with the control surfaces.

Lambourne and Bryer (1961)⁵ described vortex breakdown as a structural change at some position along a vortex from a strong regular spiral motion to a weaker turbulent motion. There is a sudden deceleration of fluid along the vortex axis and expansion of the vortex around a stagnant core downstream of which the flow is turbulent and resembles the wake behind a solid object. Lambourne and Bryer observed two distinctive types of breakdown, a bubble and a spiral, both of which are illustrated in Figure 1.2.

The bubble breakdown is characterized by a stagnation point on the vortex axis followed by an oval shaped recirculation zone. The upstream half of the recirculation zone can be nearly axisymmetric with the flow passing smoothly around it, however the downstream half is usually open and irregular with the flow shedding from the aft end as if from a blunt solid body. The bubble is usually two to three (upstream) core diameters in length. Downstream of the bubble the vortex is turbulent and diffuses rapidly with distance.

The spiral breakdown is characterized by a rapid deceleration of the core flow followed by an abrupt kink at which point the core flow takes the form of a spiral which persists for one or two turns before breaking up into large scale turbulence. The spiral is also

rotating and, for leading edge vortices, the rotation of the spiral is in the same direction as the rotation of the upstream vortex, while the sense of the spiral is opposite to the direction of rotation.

1.4 Objectives

Under sponsorship of the NASA Ames Research Center the authors of this report conducted experimental studies to examine the leading edge vortex flows on a family of flat plate delta wings. The objective of this research effort was to improve the basic understanding of vortex breakdown. Experimental data was obtained using seven-hole pressure probes, laser Doppler anemometry and flow visualization. Much of the quantitative information such as the flow surveys have been reported in a number of papers and journal articles.⁶⁻¹¹ Although some of the flow visualization results were included in these papers it was felt that a comprehensive presentation of the flow visualization results in a single report would be useful to both experimentalist and theoreticians studying leading edge vortex flows. After reviewing literally thousands of photographs, the following collection of photographs were selected. The authors hope that these photographs will provide insight into this complex fluid mechanics problem.

EXPERIMENTAL APPARATUS

2.1 Wind Tunnel

All experiments were conducted in the University of Notre Dame's low turbulence, subsonic wind tunnel. The tunnel is of the indraft (open circuit) type as shown in Figure 2.1. Twelve anti-turbulence screens are located at the inlet just upstream of a 24:1 area contraction cone. The combination of anti-turbulence screens and the large inlet contraction provides a uniform velocity profile with a turbulence intensity of less than 0.1% in the test section. The test section is 183cm (6ft) long with a 61 x 61cm (2 x 2ft) square cross section. The test section was designed with large plate glass windows in the top and both sides to provide adequate viewing area for the visualization studies. Downstream of the test section the flow is expanded in a diffuser. The tunnel is powered by an eight-bladed fan and an 18.6kw AC induction motor located at the end of the diffuser section. The flow is exhausted to the outside of the building which is necessary to remove flow visualization tracer particles but also permits atmospheric disturbances (wind gusts) to affect the flow. For this reason one or more flow restrictors are generally inserted downstream of the test section when a test is run at low speeds (less than 7.6 m/s (25 ft/s)). The large pressure drop across the flow restrictor, which consists of a square box filled with ordinary drinking straws held in place by screens at either end, reduces the affect of outside disturbances on the flow in the test section.

2.2 Models

Four thin sharp-edged delta wings were used in this study. The models each had a root chord of 406.4mm (16in) and were 6.4mm (0.25 in) thick with sweep angles of 70°, 75°, 80°, and 85°. The leading edge was beveled with a 25° angle so that a sharp edge was formed on the upper side of the model. The models used in the flow visualization tests, which were run at low speeds, were made of plexiglass and were sting mounted to a support system that provided very little interference to the flow as shown in Figure 2.2a. At

speeds higher than about 7.6 m/s (25 ft/s) the plexiglass models were found to bend in the chordwise direction which resulted in reverse camber and a higher than indicated angle of attack. To alleviate this problem a second set of models was constructed identical to the first except that they were milled out of quarter inch aluminum plate. These models were mounted on a strut connected to the lower surface of the model as shown in Figure 2.2b.

2.3 Flow Visualization Equipment

For the flow visualization experiments smoke was generated by the flash vaporization of deodorized kerosene which was dripped onto electrically heated plates enclosed in conduits through which air was forced by a small squirrel cage blower. Figure 2.3 is a sketch of the smoke generator. The smoke was fed from the smoke generator into a smoke rake. The smoke rake consists of a heat exchanger, filter bag (for eliminating large particles), and smoke tubes. For this study the smoke was introduced via a single tube as illustrated in Figure 2.4. The smoke particle size distribution has been determined to be in the range 0.1 to 1.0 micron (Batill, et al 1981)¹².

To illuminate the smoke entrained into the leading edge vortex system a laser light source was used. During the course of the study two different lasers were used, a Lexel Model 95, 4 watt argon ion laser and a Spectra Physics Model 164, 2 watt argon ion laser. The laser beam was split with a cylindrical lens to create a thin (1-2mm) triangular light sheet having either a 20° or 60° spreading angle depending on the lens used. The light sheet was aligned either normal to the model surface or parallel with the vortices.

Both still and high speed motion picture photography was used to record the visual data. A Nikon FM2, 35mm SLR camera and Kodak Tri-X 400 ASA black-and-white print film were used for the still photographs. A Milliken DBM-5, 16mm motion picture camera was used for the high speed cinema photography. Film frame rates of 500 frames per second (shutter speed 1/1300 sec) were used with Eastman

16mm 4-X Negative high speed movie film.

To obtain information on the flow characteristics near the surface of the wings a series of tests were run using fluorescent mini-tufts following the method of Crowder (1980)¹³. For these tests the tuft material consisted of extremely fine nylon mono-filament fibers (.02mm in diameter) which had been treated with a fluorescent dye. The tufts are so thin that they are nearly invisible in ordinary light, but appear many times larger and can be easily seen and photographed when illuminated with ultraviolet light. The tufts were glued to the surface of each model at 13 mm (0.5 in) intervals with a slightly thinned nitrocellulose cement. The wings were illuminated with three 2000 watt flood lamps using Corning Glass No. 5980 filters. These filters block out all wavelengths except ultraviolet at a wavelength of approximately 360 nanometers. The ultraviolet illumination excites the fluorescent material to radiate in the visible spectrum which can then be photographed with a conventional camera and ordinary film. A Wratten 2A barrier filter is used at the camera to eliminate any ultraviolet light reflected by the model. This produces very high contrast between the fluorescent mini-tufts and the non-fluorescent background.

EXPERIMENTAL PROCEDURE AND RESULTS

3.1 Smoke Flow Visualization

When investigating a complicated and unknown flow the first step is often a flow visualization experiment. The ability to see what is happening is indispensable to understanding the processes involved. For this reason extensive flow visualization experiments were carried out to study the flow past thin sharp edged delta wings at moderate to high angles of attack. Experiments using smoke to visualize the flow were run with high intensity flood lamps to observe the global flow field and using a laser light sheet to illuminate cross sections of the flow. Fluorescent mini-tufts were used to examine the surface flow characteristics. The results were both qualitative and quantitative. Not only was the structure of the leading edge vortex and vortex breakdown examined but the location of the vortex cores were tracked for a range of model sweep angles and angles of attack. The location of vortex breakdown was also identified for the same range of parameters.

For each type of experiment four models were tested with sweep angles of 70° , 75° , 80° , and 85° at angles of attack of 10° , 20° , 30° , and 40° . The freestream velocity was 3.0 m/s (10 ft/s) for runs involving smoke and 15.2 m/s (50 ft/s) for the mini-tuft experiments since higher dynamic pressures were required for adequate tuft response. This corresponded to a chord Reynolds number of 85,000 for the smoke runs and 425,000 for the mini-tuft runs. For reasons discussed in the introduction, Reynolds number effects for thin sharp edged delta wings at these angles of attack are expected to be small.

In runs in which smoke was used, a single column of smoke was introduced at the tunnel inlet and positioned so that it would impinge on the apex of the model in the test section. The smoke then became entrained into the vortices making them visible. One consequence of running at speeds as low as 3.0 m/s (10 ft/s) was that upstream of the 24:1 contraction, the inlet air speed was less than half a foot per second. This was sufficiently slow so that buoyancy effects would deform the smoke column, which originally

had a circular cross section, into a curled u-shaped cross section as seen using the laser sheet in Figure 3.1. This had no effect on the flow but care had to be taken not to confuse the curls with flow features.

In the first set of experiments a 1000 watt flood lamp was used to illuminate the flowfield and observe the vortices. Photographs were taken of each model at the test conditions previously described (See Appendix A, Figures A1-A16). Several interesting observations were made. At the lowest angle of attack (10 degrees) the primary vortices swept along the surface of the model, as the incidence was increased the vortices lifted from the surface and became more clearly defined. At the highest angle of attack (40 degrees) vortex breakdown occurred above all the models.

In all the photographs a dark region void of smoke is seen along the axis of the vortices. This is commonly observed in flow visualization and laser Doppler anemometer experiments in which particles have been introduced into a vortical flowfield (Chigier 1974¹⁴, Anders 1982¹⁵, Vorropoulos et al 1982¹⁶). The lack of particles is possibly the result of the high circumferential velocities in the subcore region spinning most of the large particles out. Particles which remained would be further dispersed by the high axial velocities. Observations with a laser beam passed through the subcore show that even dust particles are absent.

Erickson (1981)¹ suggested another reason for the phenomenon. In his explanation, smoke introduced into the vicinity of the vortex core assumes a location along the outer edge of the viscous subcore due to the matching of pressures between the inner and outer flow regimes.

Yet another explanation is simply that most of the fluid in the core may be entrained from regions where there are no seeding particles to begin with (smoke is usually introduced in a thin column near the apex), and what few particles are entrained are greatly diffused by the high velocities in the subcore.

However, in a recent study by Visser, et al¹⁷, particles injected near the apex of the model were found to be entrained into

the vortex core. It appears that core flow comes from a very small region near the apex of the model and unless a strong concentration of particles are present the core region will look like a hole or void in the smoke flow.

Another phenomenon which was particularly visible on the 85° sweep wing is that the smoke, after becoming entrained into a vortex, would break into individual filaments and spiral downstream. The appearance of these filaments is believed to be the result of the formation of discrete streamwise vortices in the shear layer which forms the primary vortex. The significance of these discrete vortices will be discussed in more detail when the laser sheet results are presented.

Vortex breakdown was observed above all of the wings at 40° angle of attack. As expected, the breakdown occurred farther forward on the high aspect ratio (low sweep) wings. The breakdown position was relatively steady and symmetric on both sides of the 70° wing except for a high frequency low magnitude oscillation. However, with increasing sweep the breakdown locations became increasingly asymmetric and unsteady. On the 85° wing only one vortex would usually be breaking down above the wing at a time and, at low speeds, the breakdown location varied extensively over approximately 50 percent of the chord length. At a freestream velocity of 3.0 m/s (10 ft/s) the breakdown was observed to switch from side to side apparently at random. Sometimes a breakdown could be seen moving downstream along one vortex while at the same time a breakdown in the other vortex was moving upstream. However, it was discovered that this large scale migration only occurred at very low speeds and that when the freestream velocity was increased above 7 m/s the position of the breakdowns would stabilize with one vortex breaking down above the wing and the other in the wake.

The asymmetry in breakdown location on highly swept wings has been attributed to an increased sensitivity to yaw alignment (Wentz 1969)¹⁸ with as little as 1/10 of a degree of misalignment being significant for wings with sweep angles of 75° or more. The proximity of the cores on highly swept wings also results in

increased interference and interaction between neighboring breakdowns. This can account for the switching of the breakdown from one side to the other. According to Anderson (1983)¹⁹ the breakdown positions on highly swept wings are bi-stable. There is a preferred orientation with one breakdown occurring a certain distance upstream of the other but which side breaks down first is not significant and can be easily altered by pressure fluctuations.

The large scale migrations which were observed at low tunnel speeds but not at high speeds are probably the result of pressure fluctuations due to external wind gusts becoming significant at the low speeds. The open circuit wind tunnel used for these experiments vented to the outside of the building and therefore was susceptible to this type of interference.

The high frequency, low amplitude oscillations which were observed at all tunnel speeds are a well known feature of vortex breakdowns and have been observed both on delta wings (Lowson 1964¹⁷, Erickson 1980¹) and in vortex tubes (Sarpkaya 1971^{21,22}, Faler 1977^{23,24}). In the latter experiments this unsteadiness was observed even in carefully controlled situations in which every effort was made to insure steady flow conditions.

3.2 Laser Light Sheet Technique

The second set of flow visualization experiments involved the laser light sheet technique (Figure 3.2). The beam from a 4 Watt argon ion laser was passed through a cylindrical lens and split into a plane or sheet of light. The light sheet then passed through the test section illuminating a cross section of the flow. The flowfield was made visible by the introduction of smoke which is entrained into the vortices. The light sheet could be oriented either perpendicular to or parallel with the model. The flow was then photographed using a Nikon FM2 35mm camera using Kodak Tri-X black-and-white film or Kodak Ektachrome color slide film.

The photographs obtained using this technique for the four models and four angles of attack tested are presented in Appendix A. Figures A17-A32 are lateral cross sectional views (light sheet

perpendicular to the model) and Figures A33-A48 are longitudinal cross sections (light sheet parallel with the model). The lateral cross sections are multiple exposure photographs obtained by taking an exposure, then moving the light sheet to the next station and taking another exposure without advancing the film and so on until all five stations had been photographed. The stations were evenly spaced at $x/c = 0.167, 0.333, 0.500, 0.667, \text{ and } 0.833$.

Figures A17-A20 are the lateral cross section photographs for the 70° wing. The feeding sheets and vortices are clearly visible although the cores are rather diffuse and featureless except for the presence of the subcore which is dark and void of smoke. The cores grow in size as the angle of attack is increased until at 40° vortex breakdown occurs somewhere between the second ($x/c = 0.333$) and third ($x/c = 0.500$) stations. The approximate breakdown location is identifiable in the photographs by the disappearance of the dark subcore region and by the turbulent nature of the vortex cores downstream of the second station.

The lateral cross sections for the 75° and 80° wings are presented in Figures A21-A28. On these wings vortex breakdown is seen to occur somewhere between the third and fifth stations with breakdown occurring earlier in one vortex than in the other on both wings.

Figures A29-A32 are the lateral cross section photographs for the 85° wing. The vortex cores in these photographs are exceptionally clear and details of the secondary structure in the shear layer are visible. At 10° angle of attack the shear layer winds smoothly into the vortex core. The double curls above the center of the model are a remnant of the smoke column as explained in the previous section and are not flow features.

As the angle of attack is increased to 20° (Figure A30) vortical structures appear in the shear layer and develop in a manner similar to a Kelvin-Helmholtz instability. At 30° angle of attack (Figure A31) the left vortex has become turbulent and details are no longer apparent, but the secondary structure is visible in the right vortex. At 40° angle of attack (Figure A32)

structure in the shear layer is still visible and vortex breakdown occurs in the left vortex aft of the third station.

Details of the secondary structure in the shear layer are visible in photographs presented in Figure 3.3 which are lateral laser sheet cross sections of the vortex at $x/c = 0.667$ and $x/c = 0.833$ on the 85° wing at 30° angle of attack. The secondary structure is seen to consist of small streamwise vortices in the shear layer. The presence of tiny subcore regions can clearly be seen in the photographs. These are the cross sections of the vortex filaments observed in the smoke flow visualization photographs described in the previous section.

It is interesting to note that when the smoke stream drifted away from the apex of the wing it was sometimes entrained into the region in between the feeding sheet and the core. When this occurred the shear layer vortices appeared as dark areas void of smoke but still identifiable by their outlines (Figure 3.4). This is further evidence that the structure is real and not a consequence of the flow visualization method.

The existence of small streamwise vortices in separated vortex sheets was previously suggested by Squire (1961)²⁵. Squire observed streamwise lines in oil flow visualization experiments and "jagged edges" in vapour-screen photographs of a 65° sweep wing at 8.2° angle of attack at high subsonic (Mach = 0.7) and supersonic (Mach = 1.5) speeds and from this evidence surmised the existence of streamwise vortices. Squire attributed the phenomenon to instability in this type of three-dimensional shear flow. A diagram of the flow with streamwise vortices from Squires paper is presented in Figure 3.5. The flow structure observed in these tests tend to confirm Squires interpretation.

It should be pointed out that the observed vortical structures are static. They do not rotate with the vortex but presumably emanate from near the leading edge and follow a spiral path which is fixed with respect to the shear layer. This is a different phenomenon from that reported by Gad-el-Hak and Blackwelder (1985)²⁶. Gad-el-Hak reported discrete vortices which shed

dynamically from the leading edge of a 60° delta wing in a towing tank experiment and appeared to pair off as they were entrained into the vortex.

A photograph depicting a two dimensional shear layer rolling up coincident with the formation of secondary vortical structures in the shear layer has been published by Batchelor (1967)²⁷. In this case the shear layer is generated by an axisymmetric body with a sharp protruding edge accelerating rapidly through a fluid at rest. The photograph shows the development a Kelvin-Helmholtz type instability in a shear layer which is itself rolling up into a spiral. The similarity between this two dimensional process and the three dimensional phenomenon observed in the delta wing vortex is striking.

The shear layer vortices are visible on the 85° wing because the vortex is laminar. As the sweep angle is reduced the angle between the leading edge and the freestream is increased resulting in a stronger primary vortex with higher axial and circumferential velocities. At the freestream velocities of these experiments 3.0 m/s (10 ft/s) the vortices on the 85° wing are predominantly laminar whereas the vortices on the 70°, 75° and 80° sweep wings are turbulent. When the freestream velocity was increased in tests with the 85° sweep wing the details disappeared and the vortex cores became diffuse.

In the lateral laser sheet photograph at 40° angle of attack (Figure A32) the fourth cross section from the apex shows a ring of smoke with a greatly expanded smokeless core region indicative of vortex breakdown. Depending on the upstream placement of the smoke a cross section of a breakdown would appear as in Figure A32 or as in Figure 3.6 where the cross section shows an annular region free of smoke and a smoke filled interior. The smoke free ring is apparently a result of the core flow expanding around the recirculation zone of a bubble type breakdown.

There was no evidence of a secondary vortex in the photographs on any of the wings, however the surface boundary layer did seem to separate outboard of the primary vortex and form a separated flow

region between the initial separation point and the leading edge. This region was largest on the 70° wing and became smaller with increasing sweep. It is possible that a weak secondary vortex existed in this region but did not show up in the photographs.

Longitudinal laser sheet cross sections are presented in Figures A33-A48. In these photographs the laser sheet was parallel with the axis of the vortices and in the plane of the vortex subcores. In all of the photographs the dark subcore region along the axis of both vortices is visible over the length of the model. Vortex breakdown is clearly seen on all the wings at the highest angle of attack. A typical longitudinal cross section is shown in Figure 3.7 with a sketch identifying the flow features.

At 10° angle of attack the vortices on the 75° - 85° wings are laminar. This is also evident in the lateral cross sectional photographs for these models. However, on the 70° wing at 10° angle of attack the flow near the apex appears to be laminar but the vortices are turbulent over most of the wing. At 20° and at higher angles of attack the vortices are turbulent on all except for the 85° wing. At 40° angle of attack vortex breakdown is occurring on all the wings. The position of breakdown is nearly symmetric on the 70° wing but extremely asymmetric on the other wings. In all cases shown in Appendix A the breakdown appears to be of the bubble type. However, on the 85° wing, the breakdown sometimes seemed to briefly take the form of a spiral. Photographs showing both types of breakdown on the 85° wing are shown in Figure 3.8.

The laser light sheet technique also provided an accurate means of determining the breakdown location. The light sheet was oriented perpendicular to the model so as to provide lateral cross sections of the vortices. The sheet was then moved slowly downstream from the apex until the dark subcore was observed to suddenly expand, then disappear into turbulent mixing. In this study the breakdown location was defined as the point where the core first began to expand. By drawing a scale on the surface of the model, the location of breakdown could be estimated by reading the point at which the light sheet crossed the scale when it was at the

breakdown location. Since the breakdown was never completely steady, the mean location was chosen. In this way the position of breakdown could be determined to within 5% of the chord length. The location of breakdown versus angle of attack for the four models tested is presented in Figure 3.9.

3.3 Fluorescent Mini-Tufts

To obtain information on the flow characteristics near the surface of the wings a series of tests were run using fluorescent mini-tufts following the method of Crowder (1980)¹³. The tufts are so thin that they are nearly invisible in ordinary light, but appear many times larger and can be easily seen and photographed when illuminated with ultraviolet light. To insure free movement of the tufts a higher freestream velocity was required than was used for the smoke flow visualization runs. For this reason the mini-tuft experiments were conducted with a freestream velocity of 15.2 m/s (50 ft/s).

Fluorescent mini-tuft photographs for the models and conditions tested are presented in Appendix A, Figures A49-A64. The mini-tufts indicate the general direction of flow on the surface, however the resolution of the tuft grid was insufficient to provide details especially on the more highly swept models.

In general, the flow on all the wings behaved similarly. The flow at the center of the model moved straight downstream from the apex to the trailing edge. Left and right of the centerline the flow moved outboard over most of the wing. Along the leading edges there was a region in which the flow moved mostly downstream. This corresponds to the separated flow region observed in the laser sheet photographs.

There was little change in flow pattern with angle of attack except at 40° where considerable unsteadiness was evident. The unsteadiness resulted in double and blurred tuft images in the photographs. Although the breakdown location can not be ascertained from this type of photograph, the unsteadiness is indicative of the presence of breakdown.

3.4 High Speed Cinema

The laser light sheet technique was used in combination with a high speed motion picture camera to capture the dynamic processes involved in vortex breakdown. The breakdown phenomenon was photographed on an 85° wing at 40° angle of attack with a freestream velocity of 3.0 m/s (10 ft/s). The camera was operated at 500 frames per second with an effective shutter speed of 1/1300 of a second. Both lateral and longitudinal cross sections of a breakdown region were photographed.

As discussed in Section 3.1 the breakdown was seen to wander back and forth over about half of the chord length on the 85° swept model when the freestream velocity was 3.0 m/s (10 ft/s). Nevertheless, because the flow is laminar at these conditions, structural details are visible that otherwise could not be seen and so these conditions were chosen for the cinema photography.

The longitudinal cross sections revealed an interesting sequence of events. The flow conditions seemed to favor the formation of a bubble type breakdown. Occasionally however, the breakdown moved downstream and briefly took what appeared to be the form of a spiral before transforming back into a bubble. The bubble was sometimes nearly symmetric but often highly asymmetric and almost constantly changing. The transformation from bubble to spiral was not instantaneous but involved a continuous sequence of intermediate forms which are difficult to classify as either bubble or spiral.

In its most stable form the bubble was nearly symmetric. The upstream subcore suddenly and smoothly expanded around a hemispherical recirculation zone. The downstream end was open and what appeared to be vortex rings were shed into the wake. The shedding frequency was estimated to be about 160 Hz which matches the expected rotational frequency of the vortex under the given conditions. The bubble was single celled with the recirculating flow moving upstream along the vortex axis. This is in contrast to the double celled structure identified in vortex tube experiments

(Faler, 1977²¹). An enlargement of a "symmetric" bubble from a 16mm movie frame is shown in Figure 3.10 along with a sketch illustrating the pertinent details. Many of the details which are visible in the movie become washed out when a print is made.

The bubble was constantly oscillating. When the oscillations grew large the nearly symmetric form described above deformed and the shedding process became asymmetric. In its most asymmetric form the recirculating flow entered and exited from the side of the bubble nearly 90° from the axis as seen in the photograph and sketch in Figure 3.11.

Occasionally the breakdown moved to a more downstream position than usual. The recirculation zone would shrink and the subcore appeared to form a tight spiral which disappeared after one or two turns (Figure 3.12). This would not last long. The core flow downstream of the breakdown would seem to force its way upstream (relative to the surrounding flow) first into the recirculation zone and then move with the bubble to some upstream position. The breakdown would tend to take the form of a spiral when moving downstream and a bubble when moving upstream. This is consistent with the theory that the bubble form is favored in a more adverse pressure gradient since a more adverse gradient is also known to move the breakdown location upstream. The pressure field was changing in the test section due to wind gusts outside the building at the tunnel exit. Small wind gusts were found to significantly affect the flow in the tunnel when operating at such low speeds.

The lateral cross sections revealed features consistent with the above description. It was impossible to fix the location of the bubble in advance so it was necessary to position the light sheet at some chordwise station and wait until the bubble crossed through the light plane. The first indication of breakdown was always the sudden (symmetric) expansion of the core. In most cases the breakdown cross section appeared as a somewhat ragged circle with an interior smoke free ring. Inside this ring the flow appeared highly turbulent. This is consistent with the description of the bubble type breakdown (Figure 3.13).

Occasionally, the smoke free ring would deform and a small region (Figure 3.14) which appeared more like an irregular hole would appear and could be seen in the movie to rotate around the edge of the vortex. Presumably, this was the result of a spiral type breakdown although the "hole" was not well defined.

The characteristics of the bubble breakdown in these experiments agrees closely with Sarpkaya's (1971)²¹ description of an "axisymmetric" breakdown in a vortex tube experiment. Sarpkaya describes a toroidal vortex ring captured at the downstream end of the bubble, whose axis gyrated at regular frequency about the axis of the bubble, and was primarily responsible for the simultaneous filling and emptying of the bubble interior.

It is significant to note that the breakdown always began as an axisymmetric expansion of the subcore which was followed by a recirculation zone which varied in extent. A large recirculation region constituted a bubble type breakdown. In this case the spiral filament was so tightly wound that it appeared as though vortex rings were being shed into the wake from the aft end of the recirculation zone. When the spiral coils "relaxed" the recirculation zone became very small and the breakdown consisted of the spiral filament alone. Thus the bubble and spiral forms appear to represent the extremes of a single process rather than two distinct breakdown modes.

CONCLUSIONS

The structure of the leading edge vortex on a family of delta wings with sweep angles from 70° to 85° and at angles of attack from 10° to 40° was studied using flow visualization techniques. The flow visualization studies revealed that the structure of a leading edge vortex consists of a spiral shear layer in which secondary vortical structures form. These structures develop in a manner similar to the Kelvin-Helmholtz instability observed in two dimensional shear flows. The shear layer vortices follow a helical path and grow in the streamwise direction as they wind into the vortex core where the individual shear layers merge.

At high angles of attack, vortex breakdown was observed on all the wings tested. Both the bubble and spiral forms of breakdown were identified. The bubble and spiral types appear to represent extremes in a continuum of breakdown forms. Intermediate forms were observed which had characteristics of both types of breakdown. At low tunnel speeds the position of breakdown was highly unsteady and high speed cinema photography showed that the spiral form was favored when the breakdown was moving downstream and the bubble form when moving upstream. The recirculation zone associated with bubble type breakdowns appeared to consist of a single celled structure in contrast to the two celled bubbles observed in vortex tube experiments.

Smoke flow visualization was used to identify the vortex trajectories on each wing tested as well as to locate the position of vortex breakdown as a function of angle of attack and sweep angle. Vortex breakdown moves upstream with increasing angle of attack and with decreasing sweep angle. The location of breakdown became increasingly asymmetric with increasing sweep.

References

- ¹Erickson, G. E.: Vortex Flow Correlation. Tech. Rept. AFWAL-TR-80-3143, 1980.
- ²Peckham, D. H.; and Atkinson, S. A.: Preliminary Results of Low Speed Wind Tunnel Tests on a Gothic Wing of Aspect Ratio 1.0. A.R.C. CP-508, 1960.
- ³Peckham, D. H.: Low-Speed Wind-Tunnel Tests on a Series of Uncambered Slender Pointed Wings with Sharp Edges. A.R.C., R. & M. No. 3186, Dec. 1958.
- ⁴Elle, B. J.: An Investigation at Low Speed of the Flow Near the Apex of Thin Delta Wings with Sharp Leading Edges. A.R.C., R. & M. No. 3176, 1958.
- ⁵Lambourne, N. C.; and Bryer, D. W.: The Bursting of Leading-Edge Vortices—Some Observations and Discussion of the Phenomenon. A.R.C., R. & M. No. 3282, April 1961.
- ⁶Payne, F. M.; and Nelson, R. C.: An Experimental Investigation of Vortex Breakdown on a Delta Wing, presented at the Vortex Flow Aerodynamics Conference, NASA Langley Research Center, Hampton, Virginia, October 8-10, 1985, NASA CP-2416, vol. 1.
- ⁷Payne, F. M.; Ng, T. T.; Nelson, R. C.; and Schiff, L. B.: Visualization and Flow Surveys of the Leading Edge Vortex Structure on Delta Wing Planforms. AIAA Paper No. 86-0330, Jan. 1986.
- ⁸Payne, F. M.; Ng, T. T.; Nelson, R. C.; and Schiff, L. B.: Visualization and Wake Surveys of Vortical Flow Over a Wing. AIAA Journal, vol. 26, no. 2, 1988, pp. 137-143.
- ⁹Payne, F. M.; Ng, T. T.; and Nelson, R. C.: Experimental Study of the Velocity Field on a Delta Wing. AIAA Paper No. 87-1231, June 1987.

- ¹⁰Payne, F. M.: The Structure of Leading Edge Vortex Flows Including Vortex Breakdown. Ph.D. Dissertation, University of Notre Dame, Notre Dame, Indiana, May 1987.
- ¹¹Ng, T. T.; Nelson, R. C.; and Payne, F. M.: Flow Field Surveys of Leading Edge Vortex Flows, accepted for the AGARD Symposium on Validation of Computational Fluid Dynamics, May 2-5, 1988, Lisbon, Portugal, AGARD-CP-437, vol. 1, pp. 11-1-11-13.
- ¹²Batill S. M.; Nelson, R. C.; and Mueller, T. J.: High Speed Smoke Flow Visualization. AFWAL-TR-81-3002, March 1981.
- ¹³Crowder, J. P.: Add Fluorescent Minitufts to the Aerodynamicist's Bag of Tricks. *Astronautics and Aeronautics*, vol. 18, no. 11, 1980, pp. 54-56.
- ¹⁴Chigier, N. A.: Measurement of Vortex Breakdown Over a Delta Wing Using a Laser Anemometer. Nielson Engineering, NASA-CR-166336, 1974.
- ¹⁵Anders, K: Laser-Doppler Velocimeter (LDV) Measurements of the Velocity Field of a Leading Edge Vortex Over a Delta Wing Before and After Vortex Breakdown. Von Karman Inst. Tech. Note 142, March 1982.
- ¹⁶Vorropoulos, G.; and Wendt, J. F.: Preliminary Results of LDV Surveys in the Compressible Leading Edge Vortex of a Delta Wing. Von Karman Inst., Tech. Note 137, Aug. 1982.
- ¹⁷Visser, K. D.; Nelson, R. C.; and Ng, T. T.: Method of Cold Smoke Generation for Vortex Core Tagging. *J. Aircraft*, vol. 25, no. 11, 1988, pp. 1069-1071.
- ¹⁸Wentz, W. H., Jr.: Wind Tunnel Investigations of Vortex Breakdown on Slender Sharp-Edged Wings. Ph.D. Thesis, University of Kansas, 1969.
- ¹⁹Anderson, M. W.; Beran, P. S.; and McCann, M. K.: Vortex Breakdown Over Delta Wings. Unpublished report, Graduate Aeronautical Laboratories, California Institute of Technology, Pasadena, CA, May 1983.

- ²⁰Lowson, M. V.: Some Experiments with Vortex Breakdown. J. of the Royal Aero. Soc., vol. 68, no. 641, May 1964, pp. 343-346.
- ²¹Sarpkaya, T.: Vortex Breakdown in Swirling Conical Flows. AIAA Journal, vol. 9, no. 9, 1971, pp. 1792-1799.
- ²²Sarpkaya, T.: Effect of the Adverse Pressure Gradient on Vortex Breakdown. AIAA Journal, vol. 12, no. 5, 1974, pp. 602-607.
- ²³Faler, J. H.; and Leibovich, S.: Disrupted States of Vortex Flow and Vortex Breakdown. Phys. Fluids, vol. 20, no. 9, 1977, pp. 1385-1400.
- ²⁴Faler, J. H.; and Leibovich, S.: An Experimental Map of the Internal Structure of a Vortex Breakdown. J. Fluid Mech, vol. 86, part 2, 1978, pp. 313-335.
- ²⁵Squire, L. C.: Flow Regimes Over Delta Wings at Supersonic and Hypersonic Speeds. Aeronautical Quarterly, vol. 27, part 1, Feb. 1976, pp. 1-14.
- ²⁶Gad-el-Hak, Mohamed; and Blackwelder, Ron F.: Control of the Discrete Vortices from a Delta Wing. AIAA Journal, vol. 25, no. 8, 1987, pp. 1042-1049.
- ²⁷Batchelor, G. K.: An Introduction to Fluid Dynamics. Cambridge University Press, 1967.

LEADING EDGE VORTEX FLOWS ON A DELTA WING

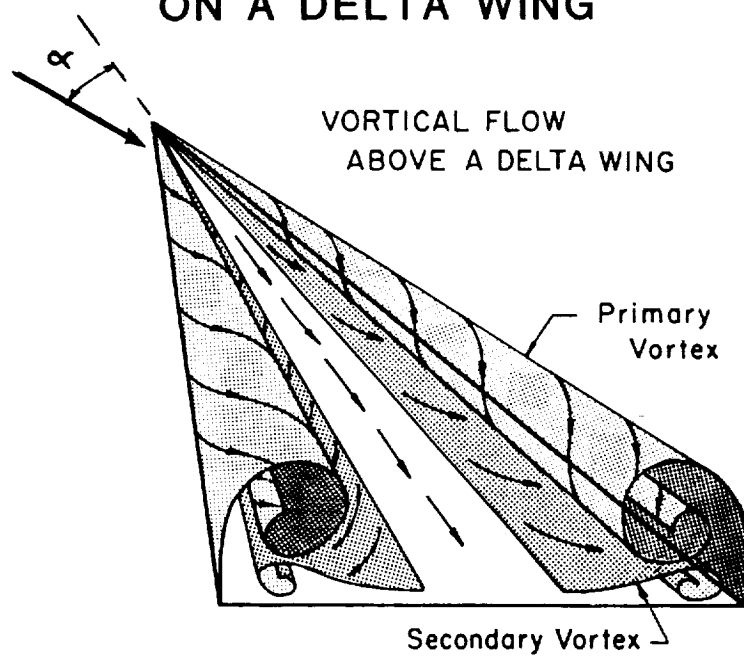


Figure 1.1 Leading edge vortex flows on a delta wing.

TYPES OF BREAKDOWN ON DELTA WINGS

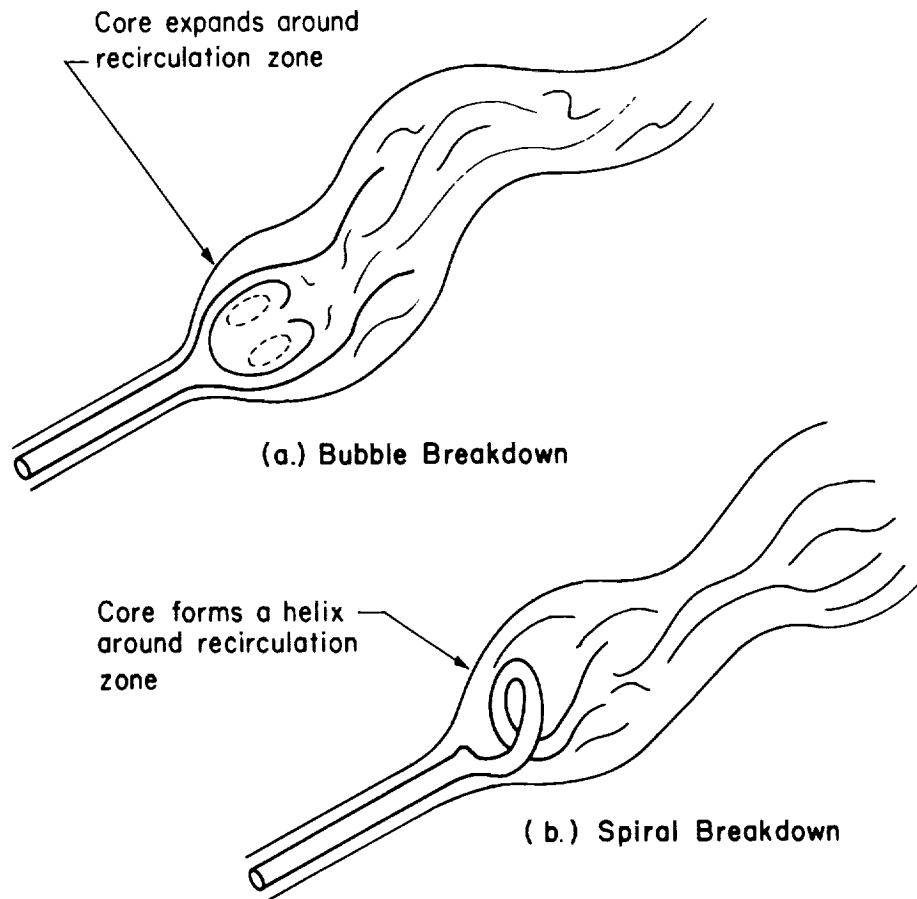


Figure 1.2 Types of breakdown on delta wings.

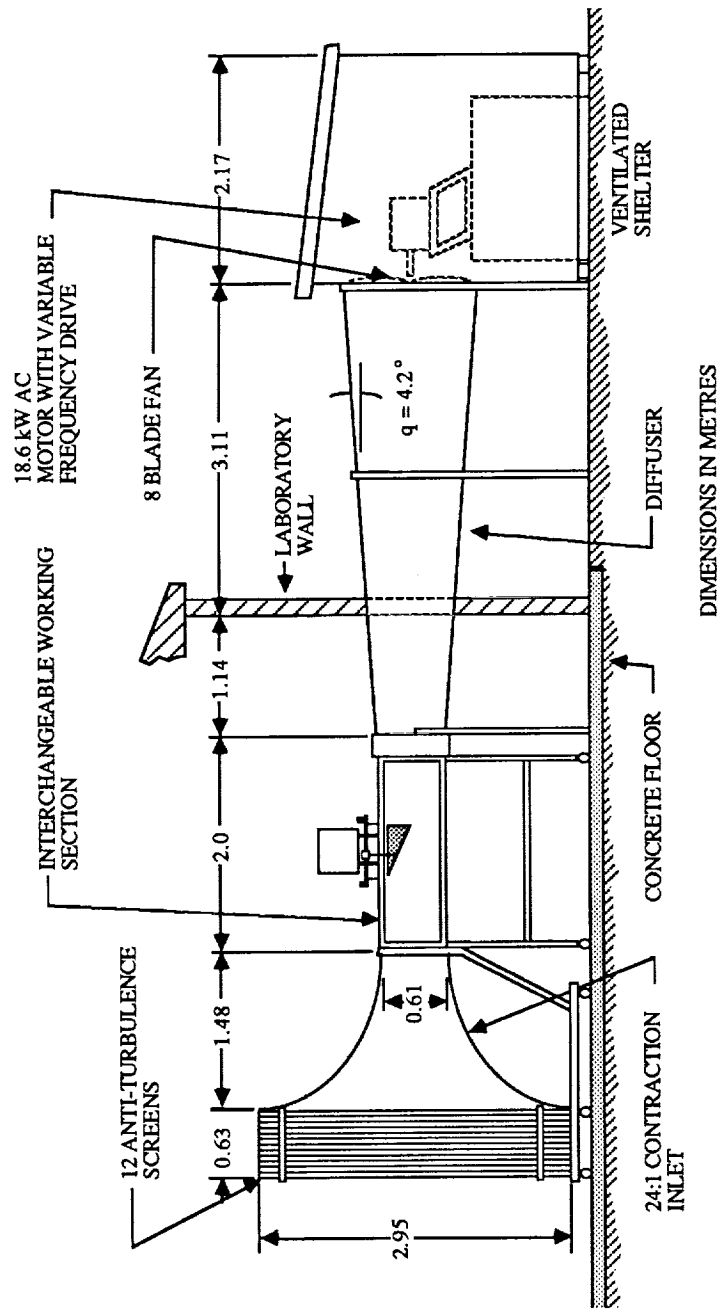
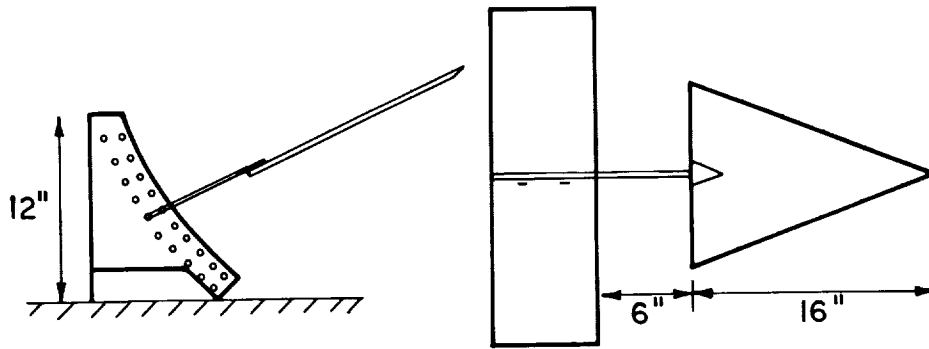


Figure 2.1 Wind tunnel

a) STING MOUNTED MODEL



b) STRUT MOUNTED MODEL

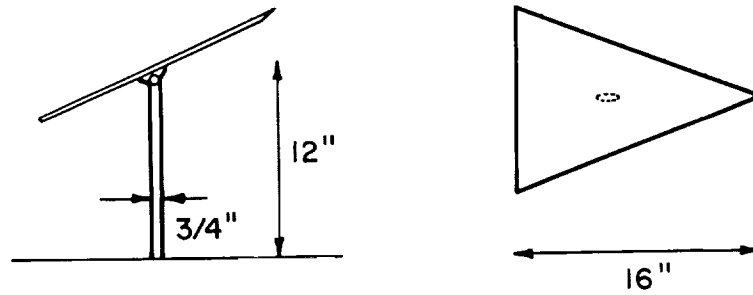


Figure 2.2 Sting and strut mounted models.

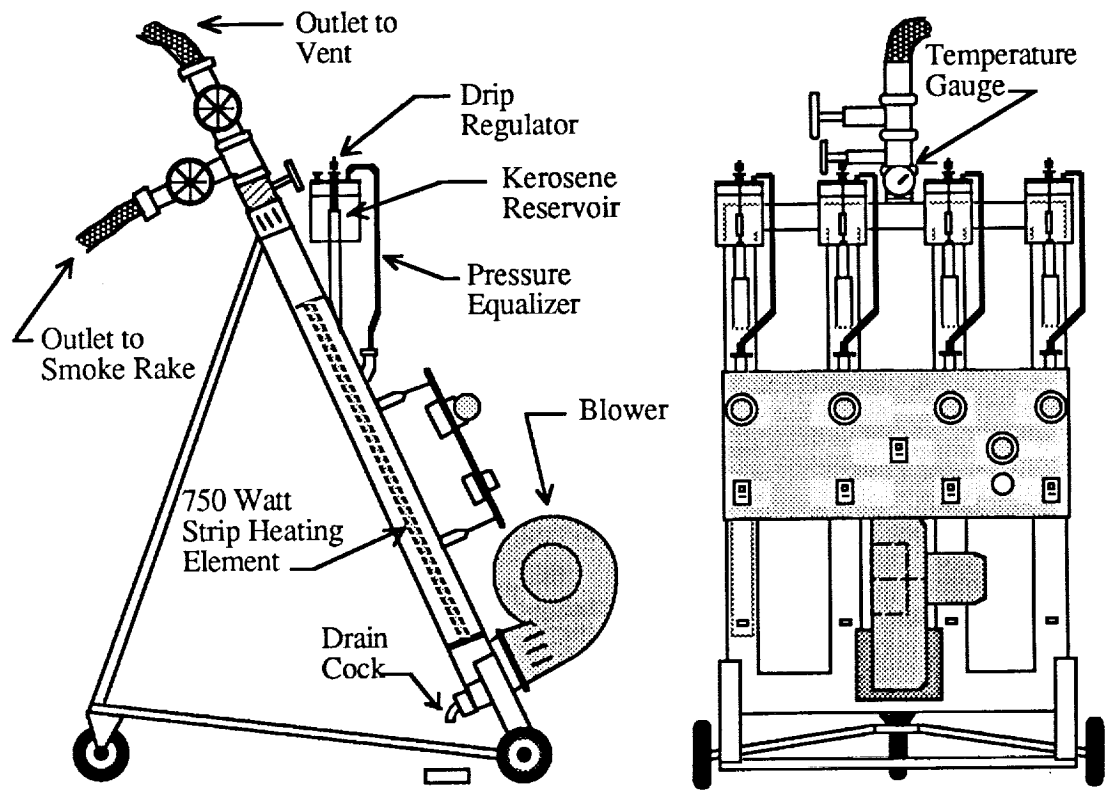


Figure 2.3 Smoke generator.

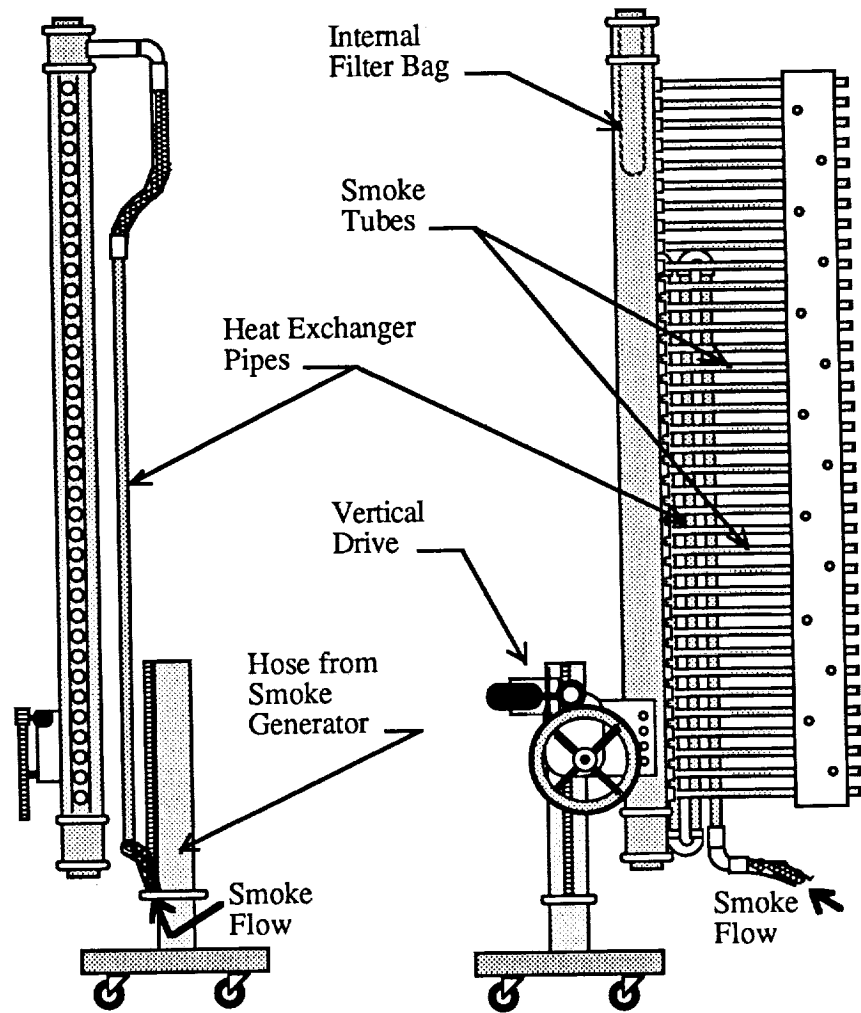


Figure 2.4 Smoke rake

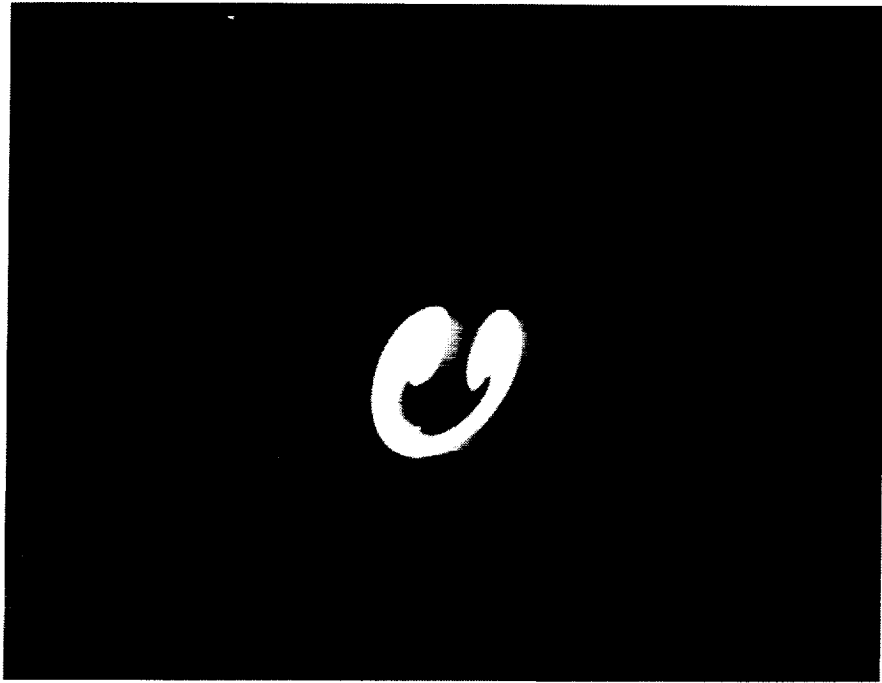


Figure 3.1 Upstream smoke tube cross section.



Figure 3.2 Schematic of laser light sheet technique.

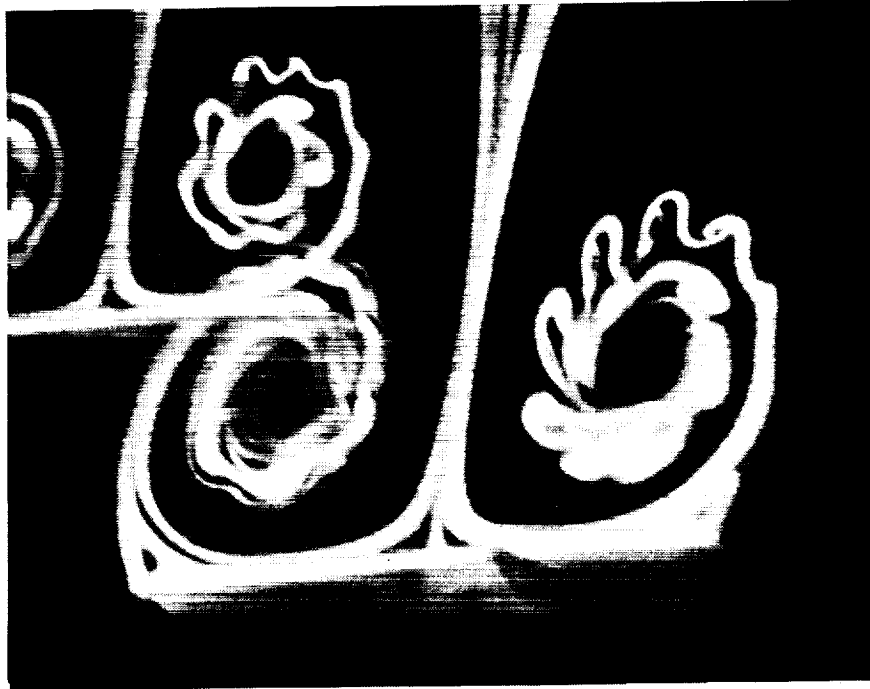


Figure 3.3 Laser sheet photographs showing secondary structure in shear layer. Sweep = 85° , Alpha = 20° , $U = 3.0$ m/s, $x/c = 0.667$ (top), $x/c = 0.833$ (bottom).

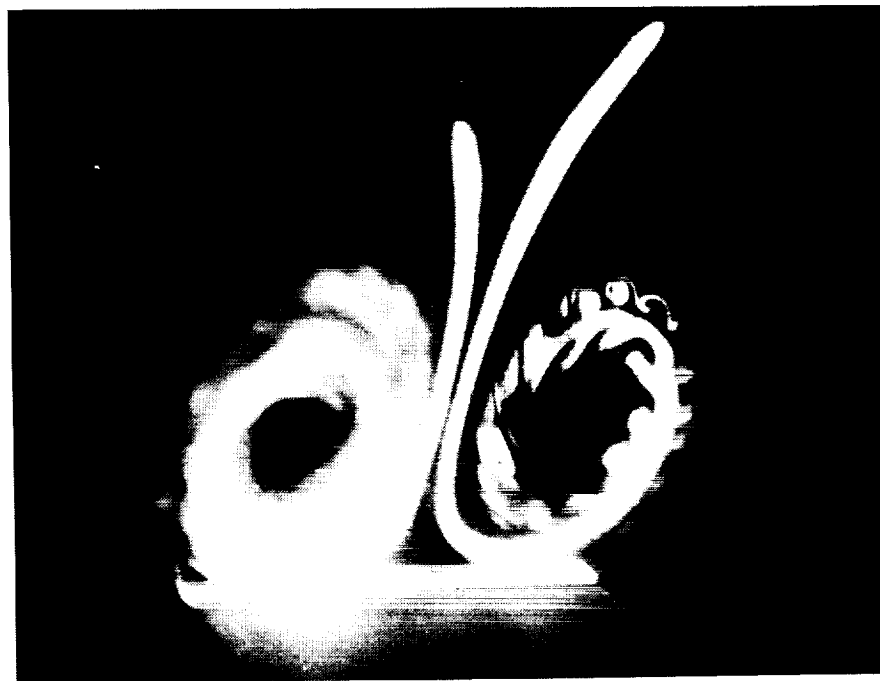


Figure 3.4 Laser sheet photograph showing outline of secondary structure in smoke. Sweep = 85° , Alpha = 20° , $U = 3.0$ m/s, $x/c = 0.667$.

DIAGRAM OF FLOW WITH STREAMWISE VORTICES VORTICES IN THE SEPARATED SHEET

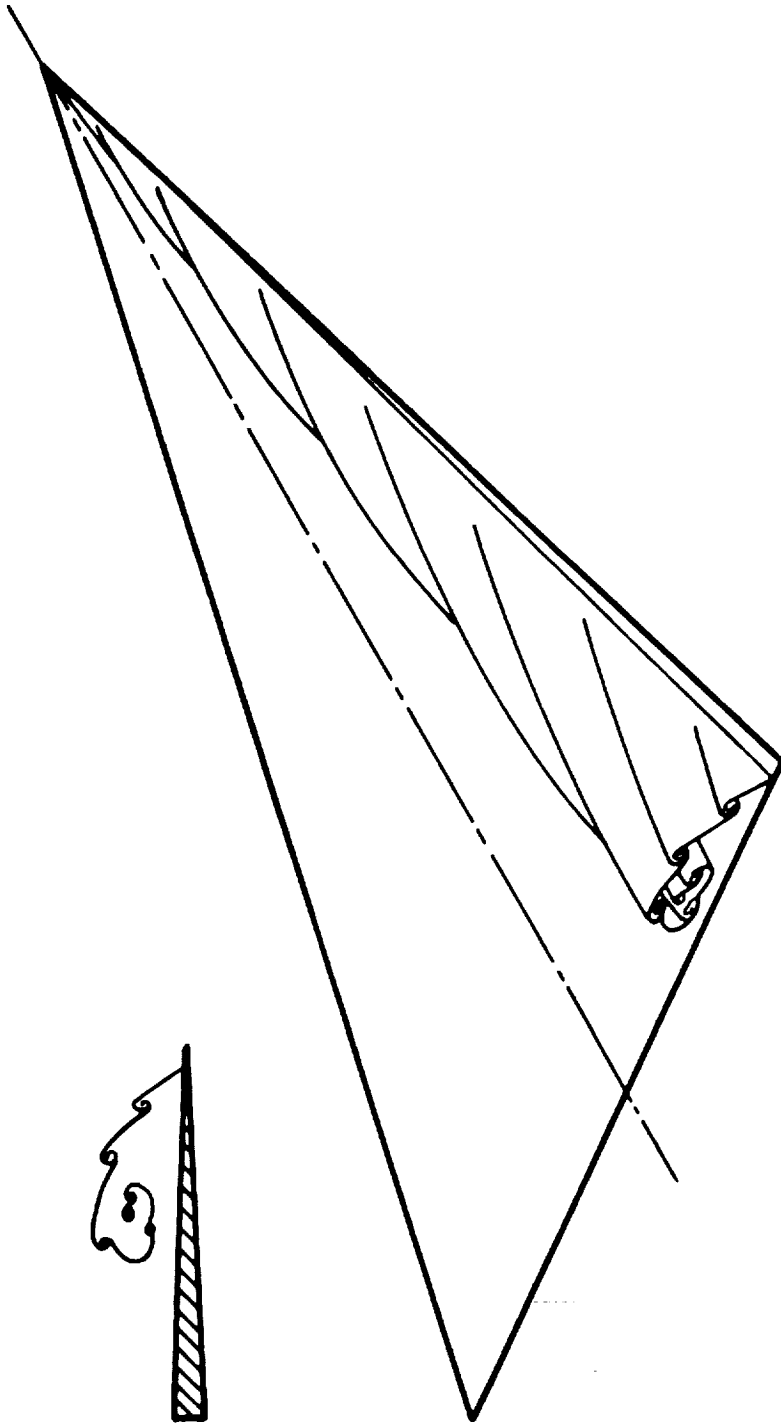


Figure 3.5 Diagram of flow with streamwise vortices.

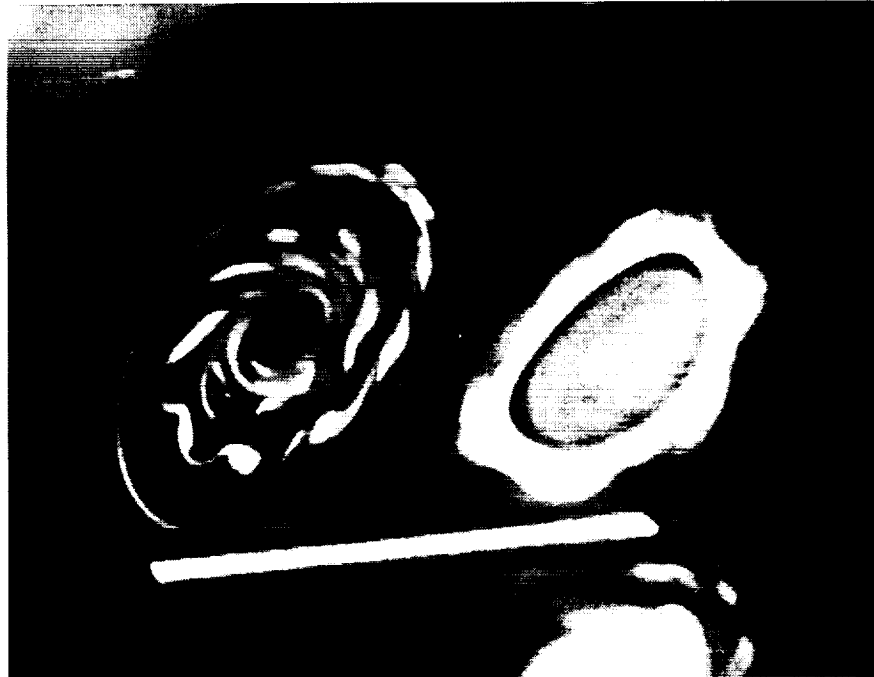


Figure 3.6 Lateral laser sheet cross section of bubble type breakdown. Sweep = 85° , Alpha = 40° , U = 3.0 m/s.

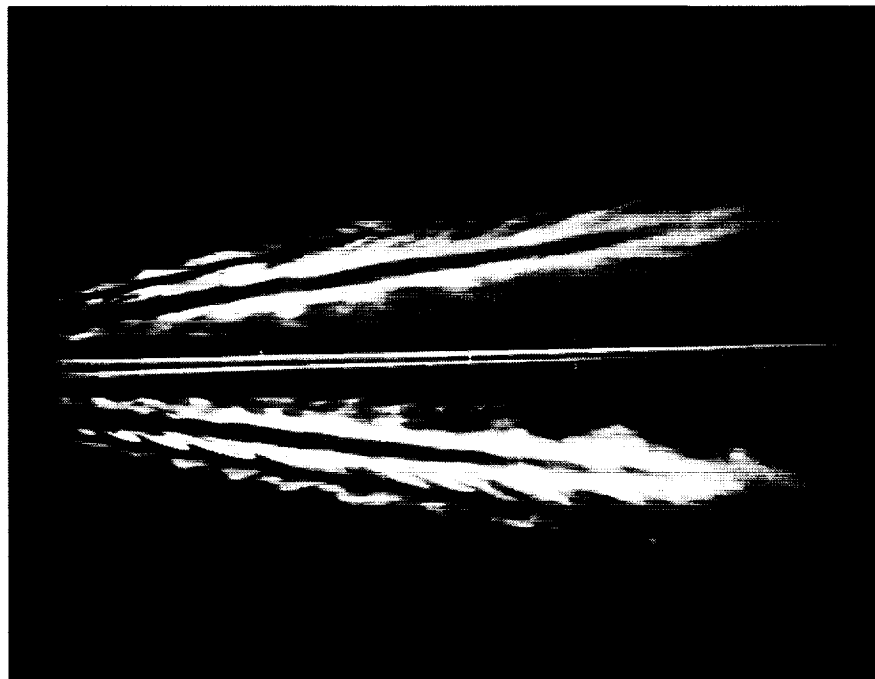


Figure 3.7 Longitudinal laser sheet cross section. Sweep = 80° , Alpha = 20° , U = 3.0 m/s.

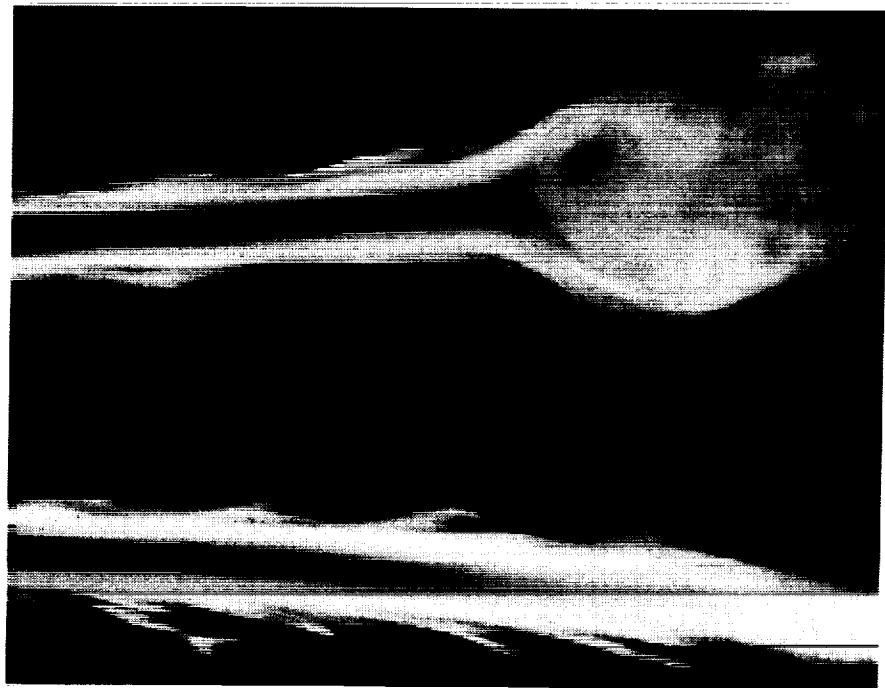


Figure 3.8 Longitudinal laser sheet cross sections of bubble type (top) and spiral type (bottom) breakdowns. Sweep = 85° , Alpha = 40° , $U = 9.1$ m/s.

LOCATION OF VORTEX BREAKDOWN
 $Re = 425,000$

- $-\Lambda = 70^\circ$
 - $-\Lambda = 75^\circ$
 - △ $-\Lambda = 80^\circ$
 - ◇ $-\Lambda = 85^\circ$
- Left Vortex
 - - - - Right Vortex

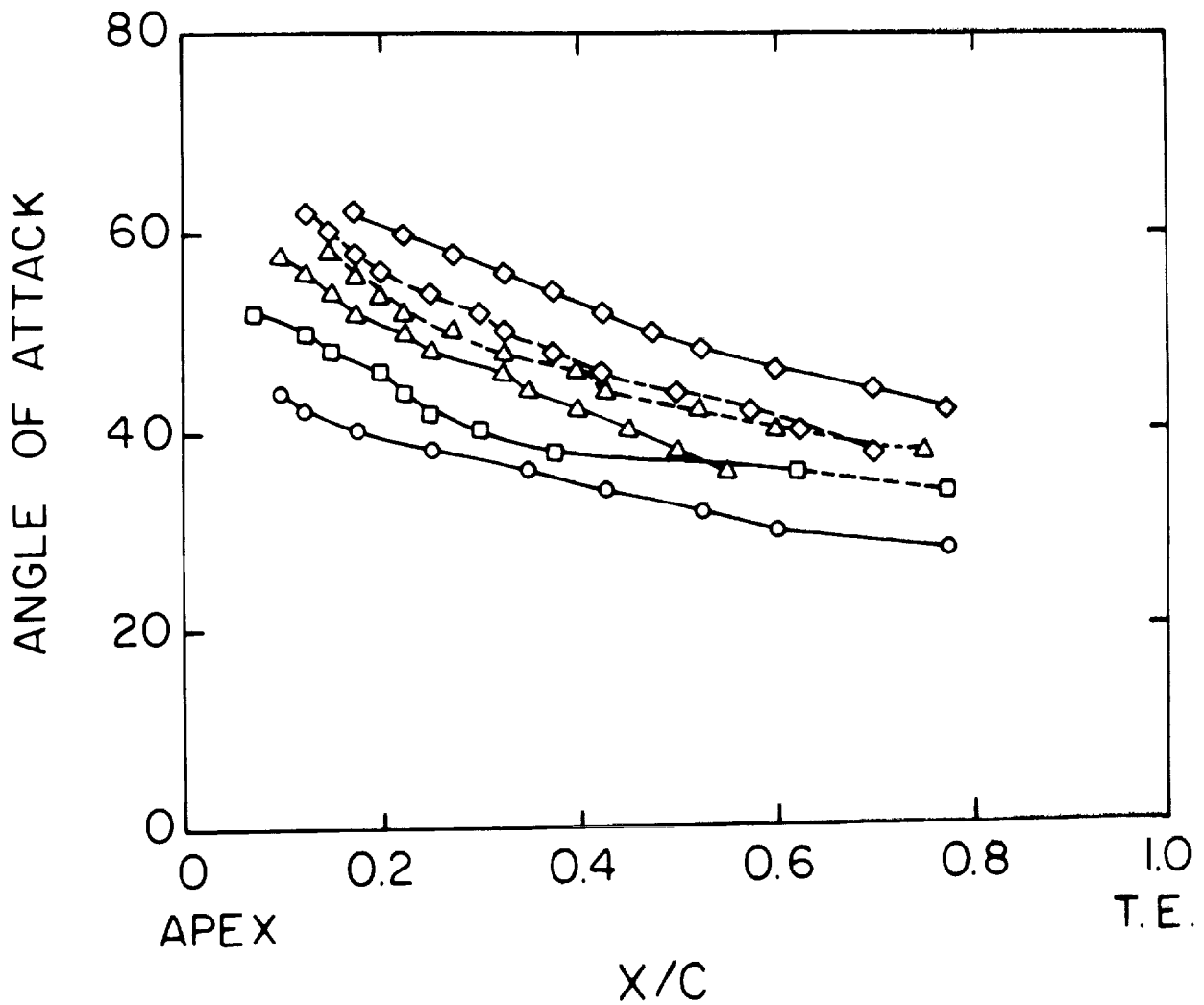


Figure 3.9 Position of vortex breakdown versus angle of attack.

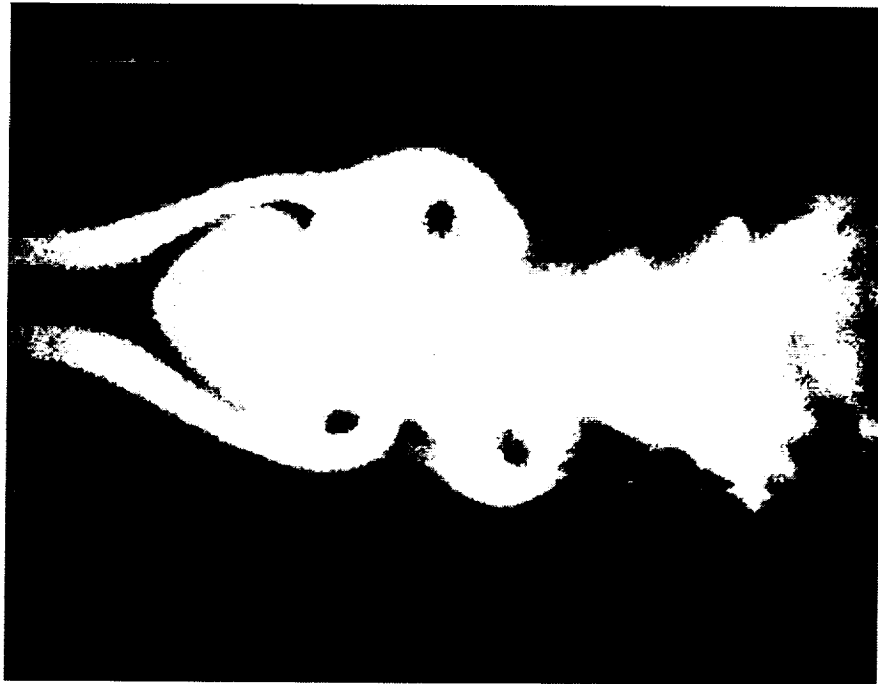


Figure 3.10 Symmetric bubble type breakdown.
Longitudinal cross section. Enlargement
of 16mm movie frame.



Figure 3.11 Asymmetric bubble type breakdown.
Longitudinal cross section. Enlargement
of 16mm movie frame.

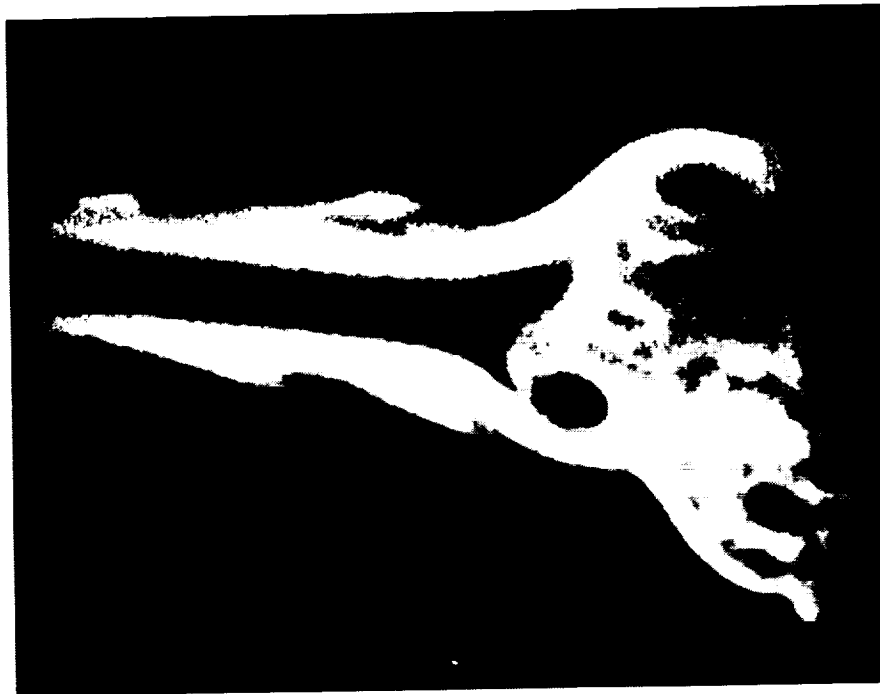


Figure 3.12 Spiral type breakdown. Longitudinal cross section. Enlargement of 16mm movie frame.

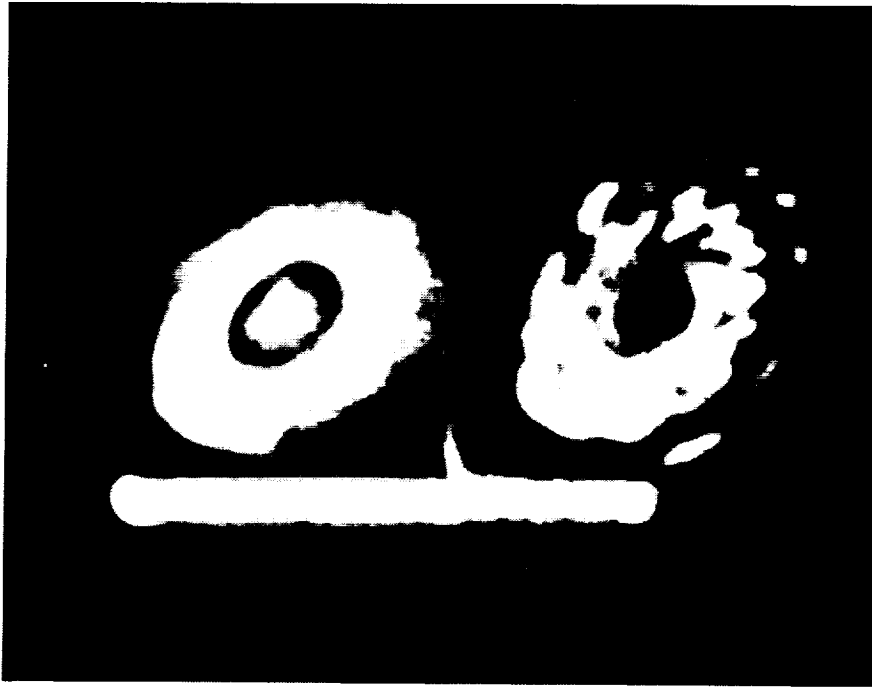


Figure 3.13 Bubble type breakdown. Lateral cross section. Enlargement of 16mm movie frame.

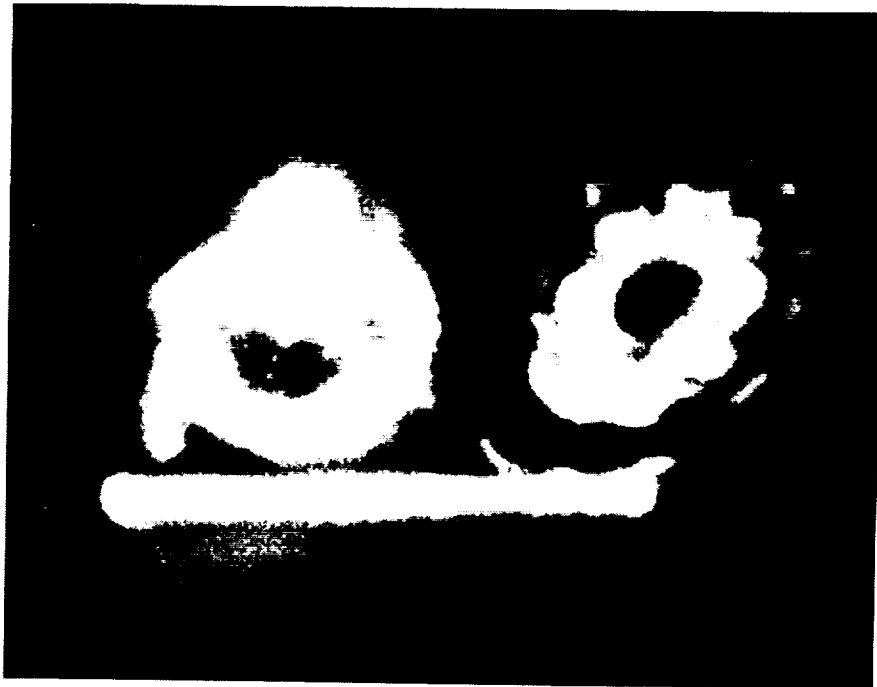


Figure 3.14 Spiral type breakdown. Lateral cross section. Enlargement of 16mm movie frame.



Figure A1. Smoke flow visualization with flood lamp illumination. Sweep = 70° , Alpha = 10° , U = 3.0 m/s.

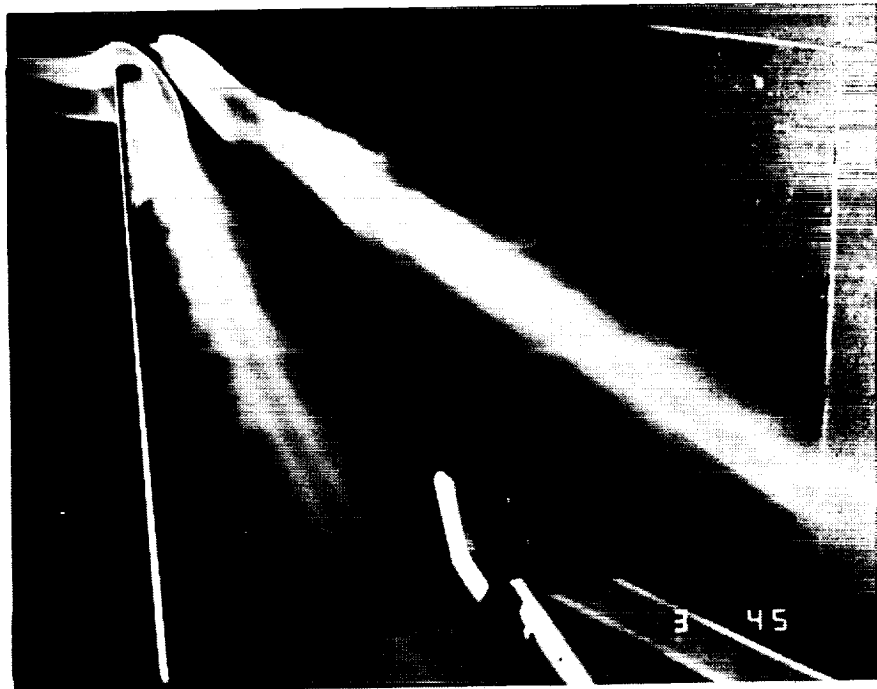


Figure A2. Smoke flow visualization with flood lamp illumination. Sweep = 70° , Alpha = 20° , U = 3.0 m/s.



Figure A3. Smoke flow visualization with flood lamp illumination. Sweep = 70° , Alpha = 30° ,
U = 3.0 m/s.

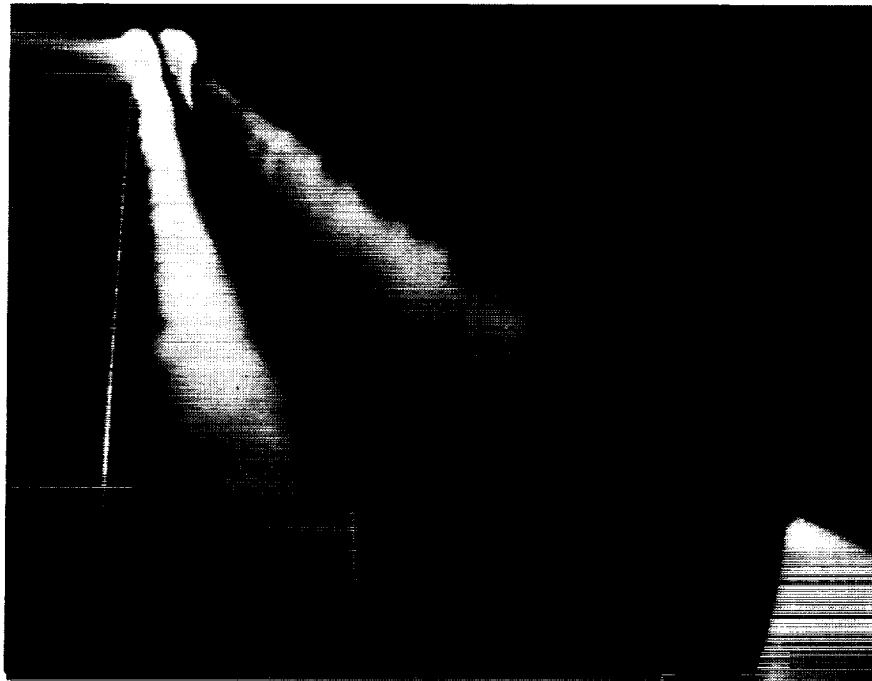


Figure A4. Smoke flow visualization with flood lamp illumination. Sweep = 70° , Alpha = 40° ,
U = 3.0 m/s.

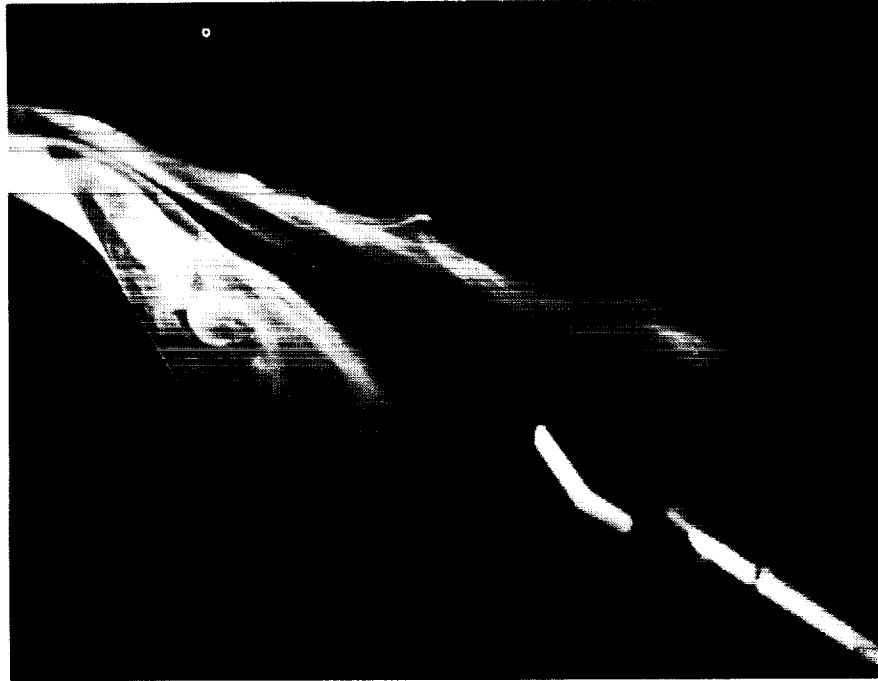


Figure A5. Smoke flow visualization with flood lamp illumination. Sweep = 75° , Alpha = 10° , $U = 3.0/s$.



Figure A6. Smoke flow visualization with flood lamp illumination. Sweep = 75° , Alpha = 20° , $U = 3.0 \text{ m/s}$.



Figure A7. Smoke flow visualization with flood lamp illumination. Sweep = 75° , Alpha = 30° , U = 3.0 m/s.

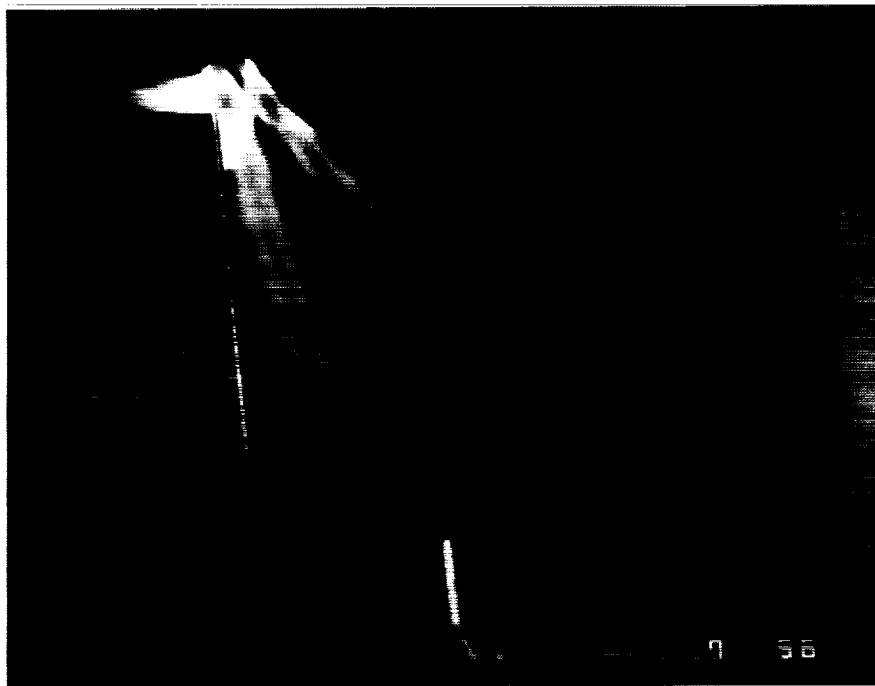


Figure A8. Smoke flow visualization with flood lamp illumination. Sweep = 75° , Alpha = 40° , U = 3.0 m/s.



Figure A9. Smoke flow visualization with flood lamp illumination. Sweep = 80° , Alpha = 10° ,
U = 3.0 m/s.

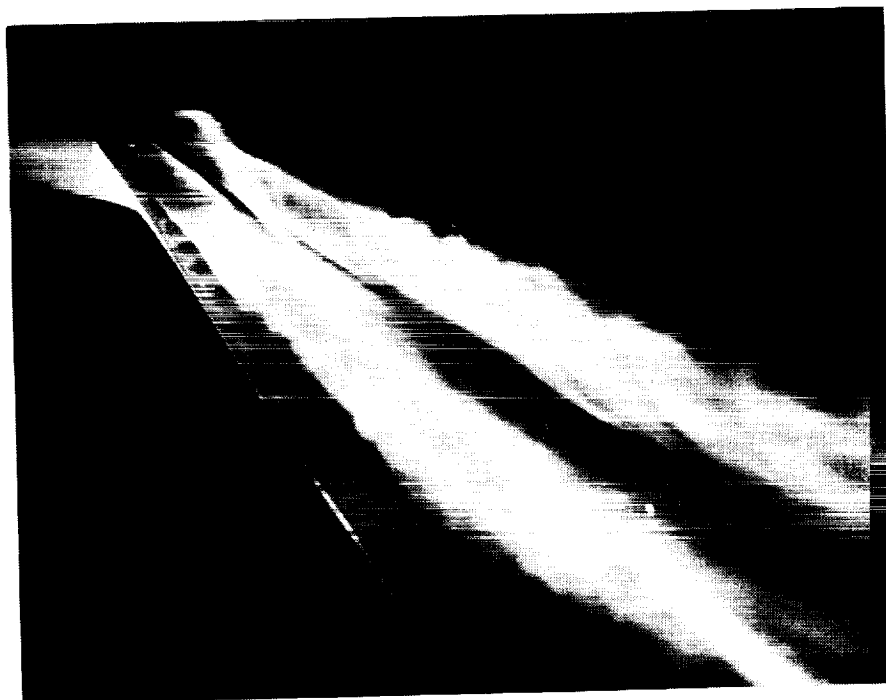


Figure A10. Smoke flow visualization with flood lamp illumination. Sweep = 80° , Alpha = 20° ,
U = 3.0 m/s.

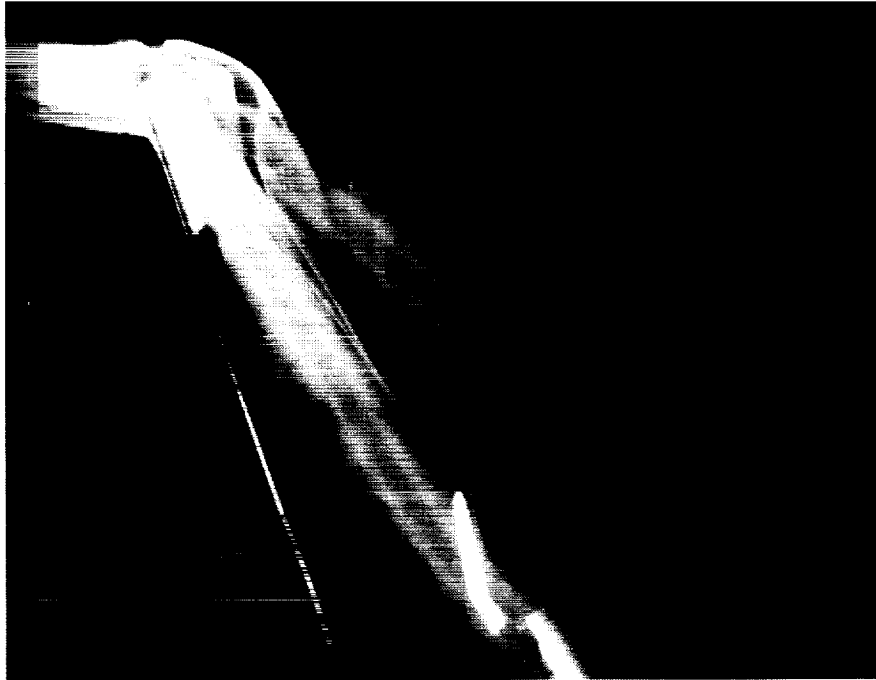


Figure A11. Smoke flow visualization with flood lamp illumination. Sweep = 80° , Alpha = 30° ,
U = 3.0 m/s.

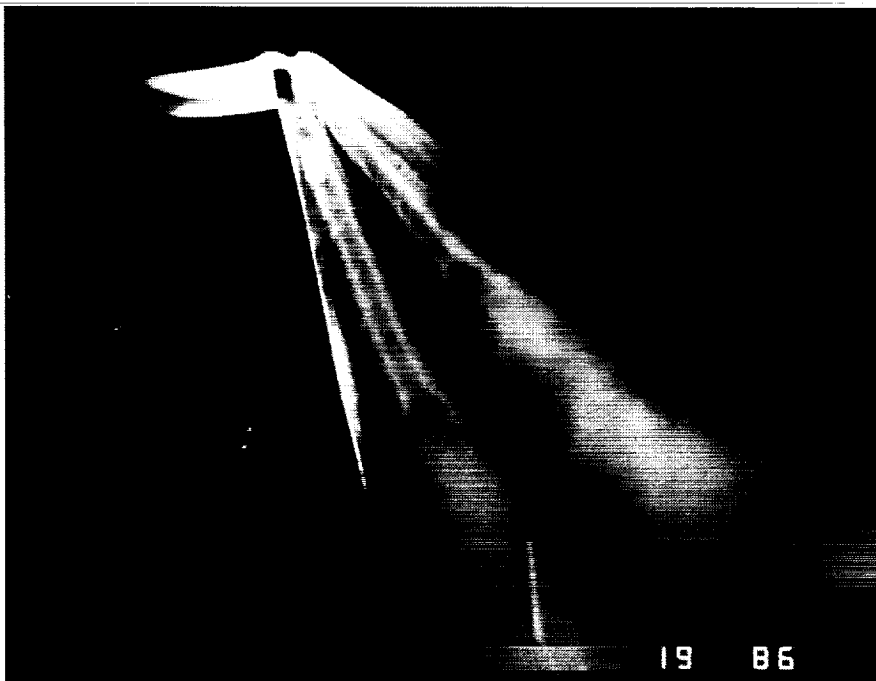


Figure A12. Smoke flow visualization with flood lamp illumination. Sweep = 80° , Alpha = 40° ,
U = 3.0 m/s.

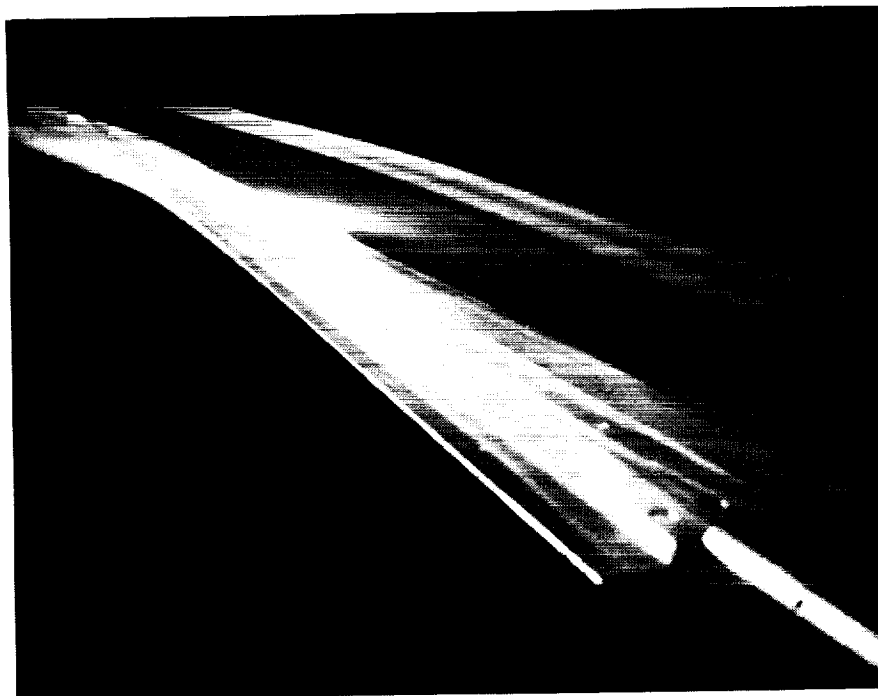


Figure A13. Smoke flow visualization with flood lamp illumination. Sweep = 85° , Alpha = 10° ,
 $U = 3.0$ m/s.



Figure A14. Smoke flow visualization with flood lamp illumination. Sweep = 85° , Alpha = 20° ,
 $U = 3.0$ m/s.



Figure A15. Smoke flow visualization with flood lamp illumination. Sweep = 85° , Alpha = 30° , $U = 3.0$ m/s.

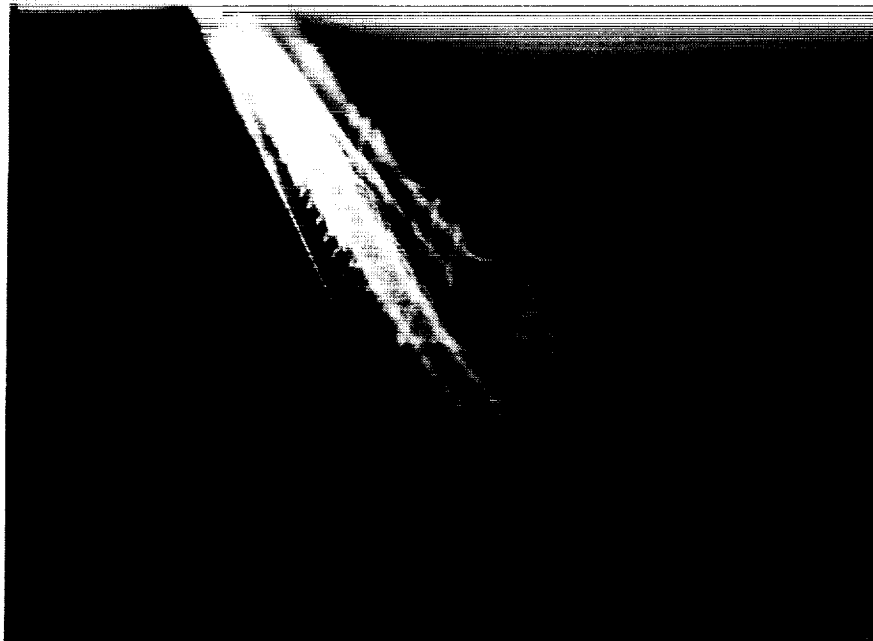


Figure A16. Smoke flow visualization with flood lamp illumination. Sweep = 85° , Alpha = 40° , $U = 3.0$ m/s.



Figure A17. Lateral laser sheet cross sections.
Sweep = 70° , Alpha = 10° , U = 3.0 m/s.

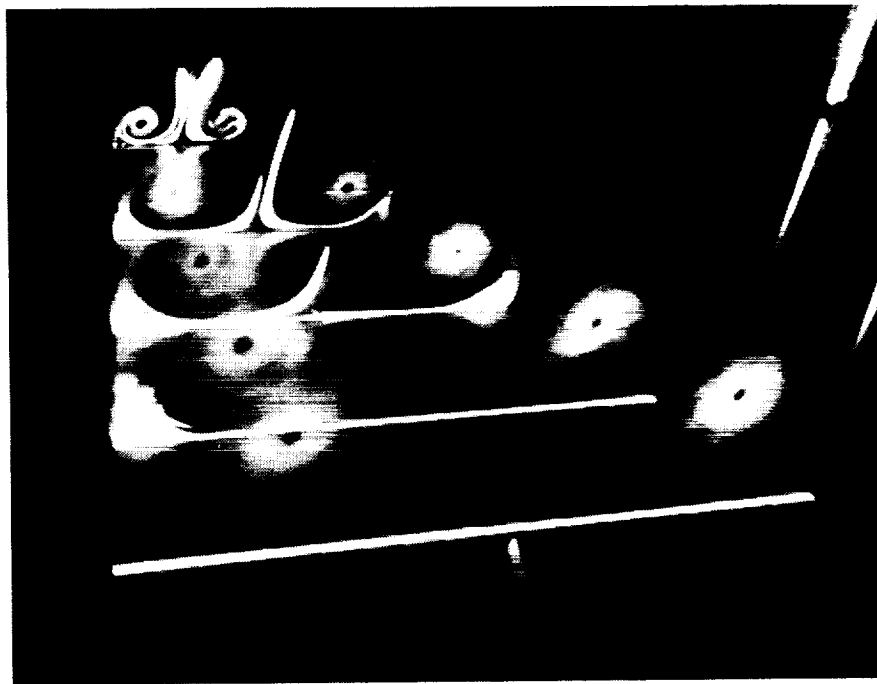


Figure A18. Lateral laser sheet cross sections.
Sweep = 70° , Alpha = 20° , U = 3.0 m/s.

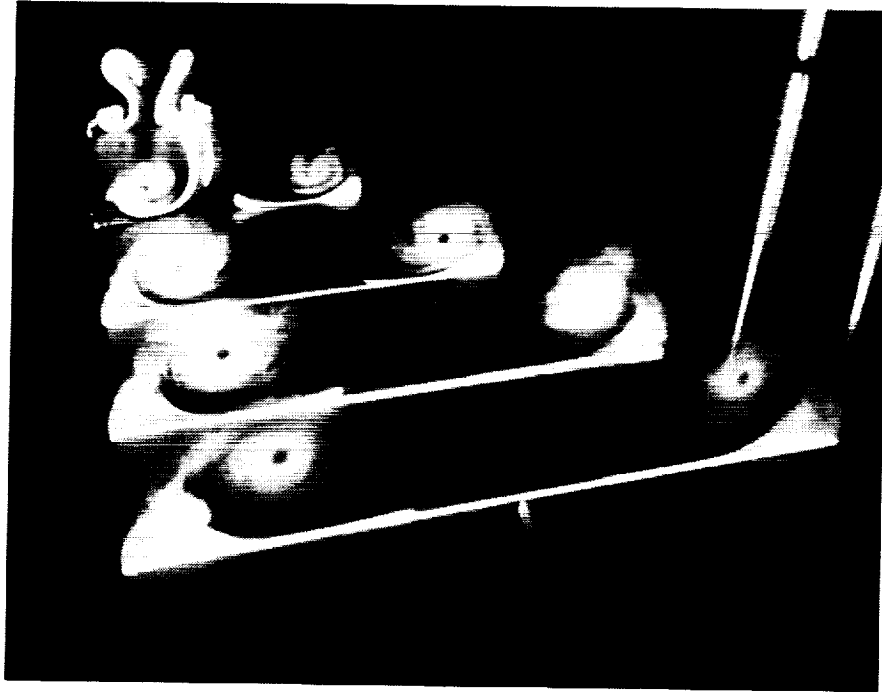


Figure A19. Lateral laser sheet cross sections.
Sweep = 70° , Alpha = 30° , U = 3.0 m/s.

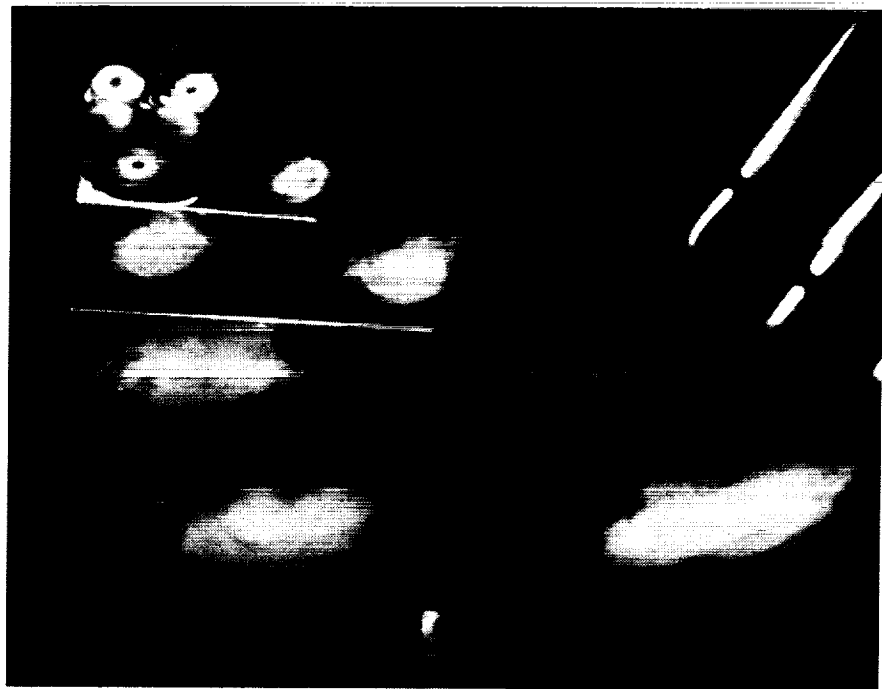


Figure A20. Lateral laser sheet cross sections.
Sweep = 70° , Alpha = 40° , U = 3.0 m/s.

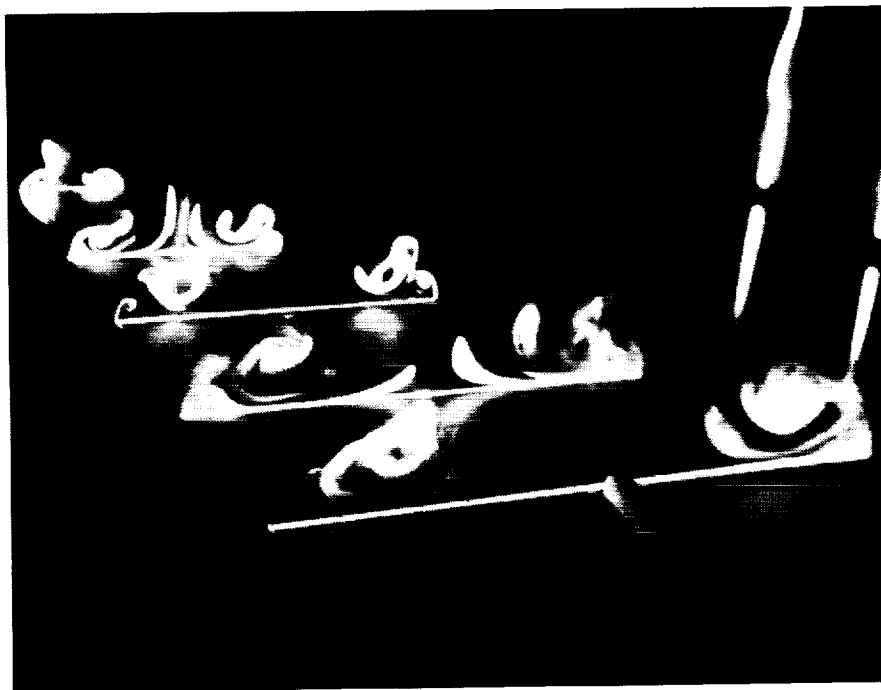


Figure A21. Lateral laser sheet cross sections.
Sweep = 75° , Alpha = 10° , U = 3.0 m/s.

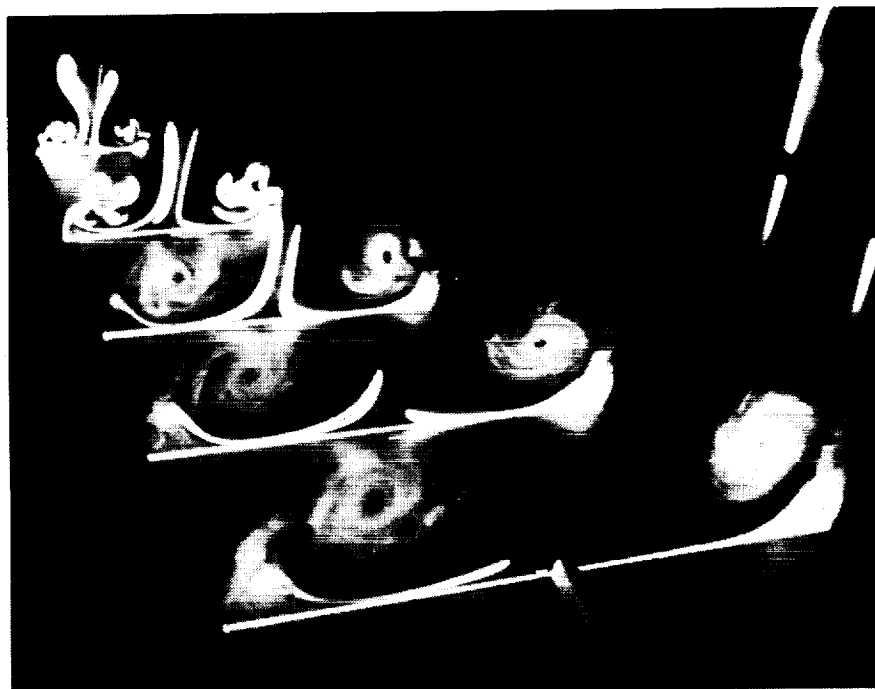


Figure A22. Lateral laser sheet cross sections.
Sweep = 75° , Alpha = 20° , U = 3.0 m/s.

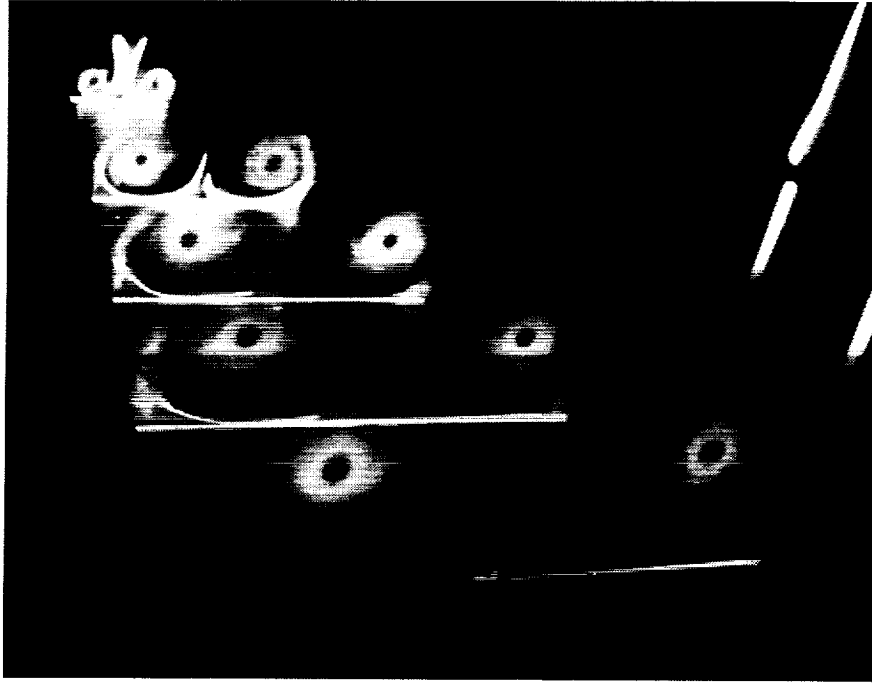


Figure A23. Lateral laser sheet cross sections.
Sweep = 75° , Alpha = 30° , U = 3.0 m/s.

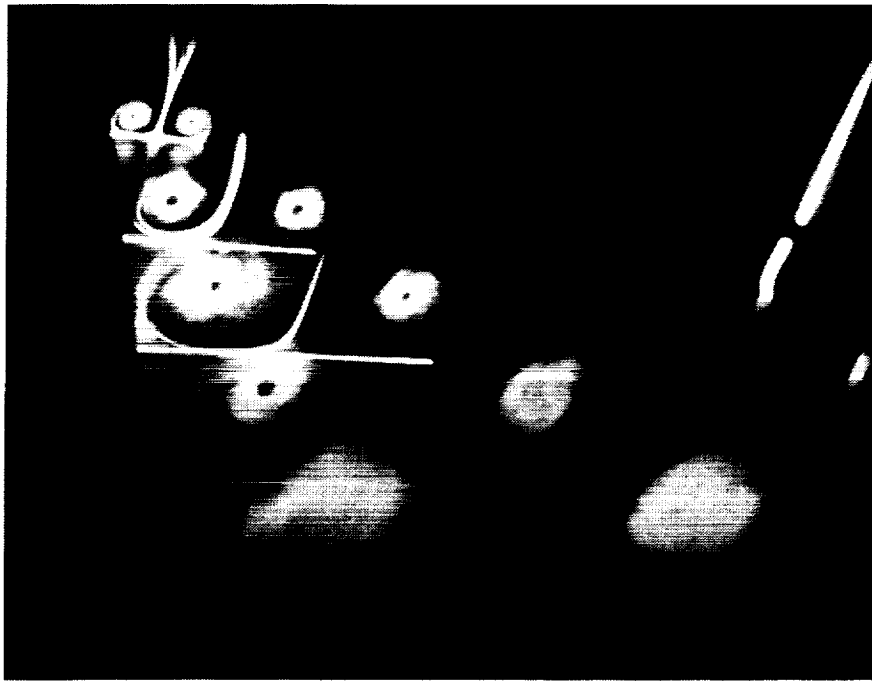


Figure A24. Lateral laser sheet cross sections.
Sweep = 75° , Alpha = 40° , U = 3.0 m/s.



Figure A25. Lateral laser sheet cross sections.
Sweep = 80° , Alpha = 10° , $U = 3.0$ m/s.

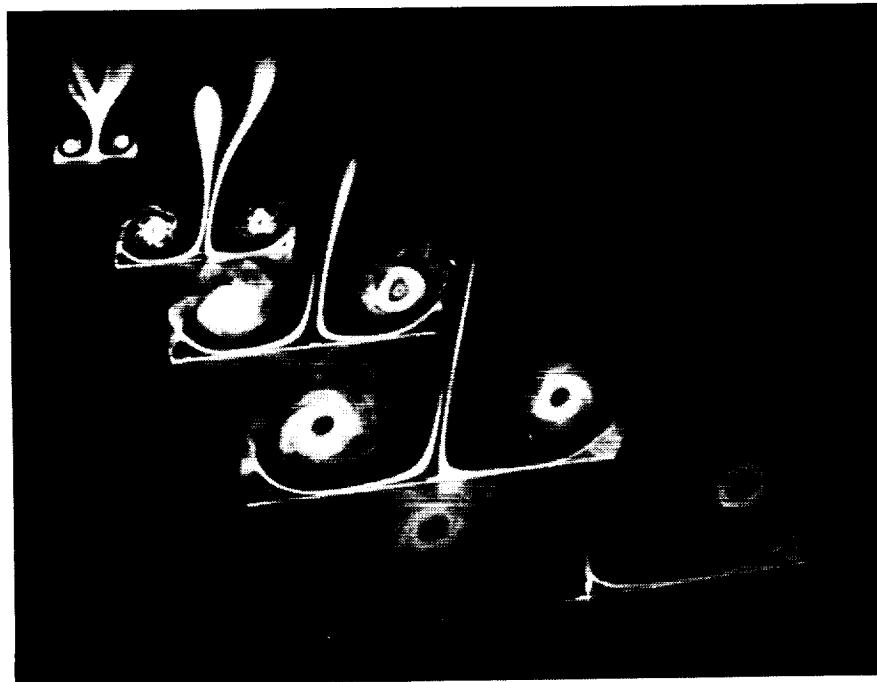


Figure A26. Lateral laser sheet cross sections.
Sweep = 80° , Alpha = 20° , $U = 3.0$ m/s.

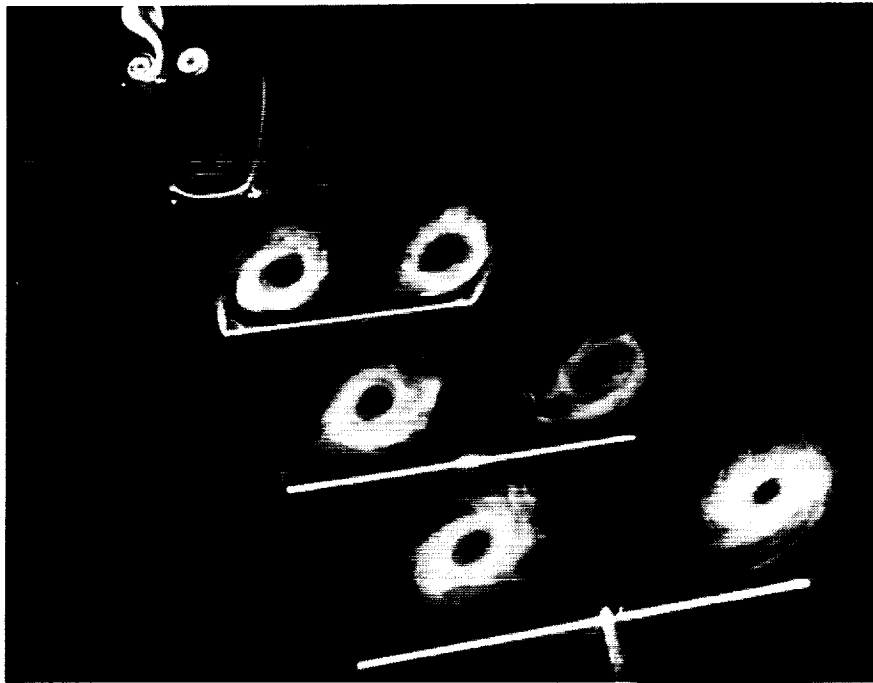


Figure A27. Lateral laser sheet cross sections.
Sweep = 80° , Alpha = 30° , U = 3.0 m/s.



Figure A28. Lateral laser sheet cross sections.
Sweep = 80° , Alpha = 40° , U = 3.0 m/s.

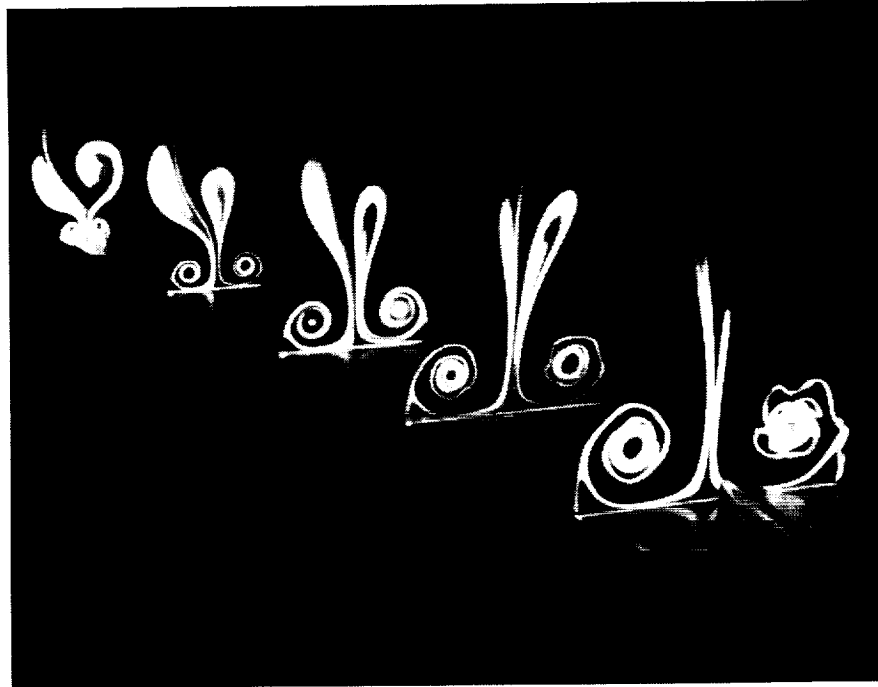


Figure A29. Lateral laser sheet cross sections.
Sweep = 85°, Alpha = 10°, U = 3.0 m/s.

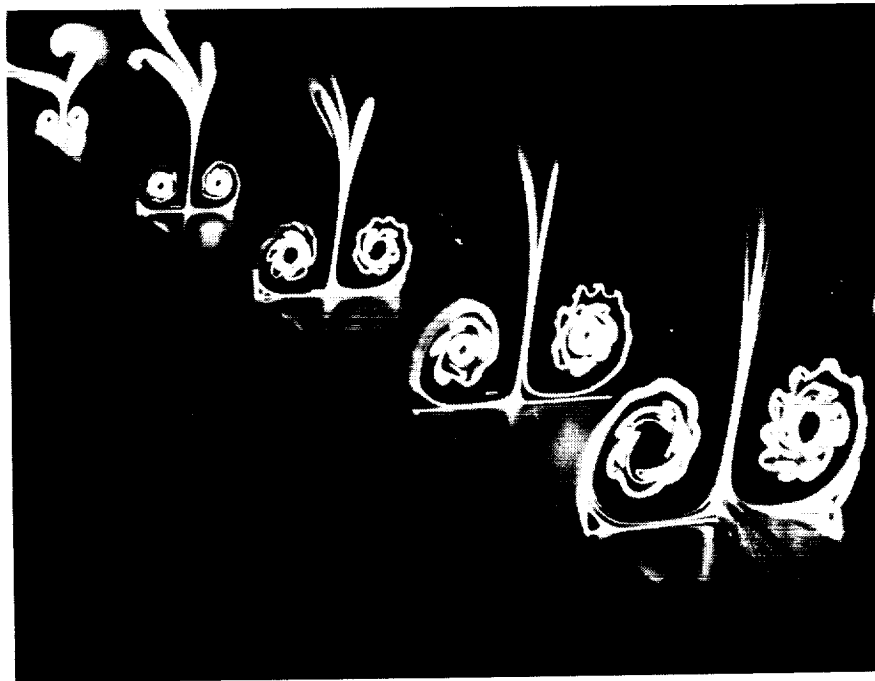


Figure A30. Lateral laser sheet cross sections.
Sweep = 85°, Alpha = 20°, U = 3.0 m/s.

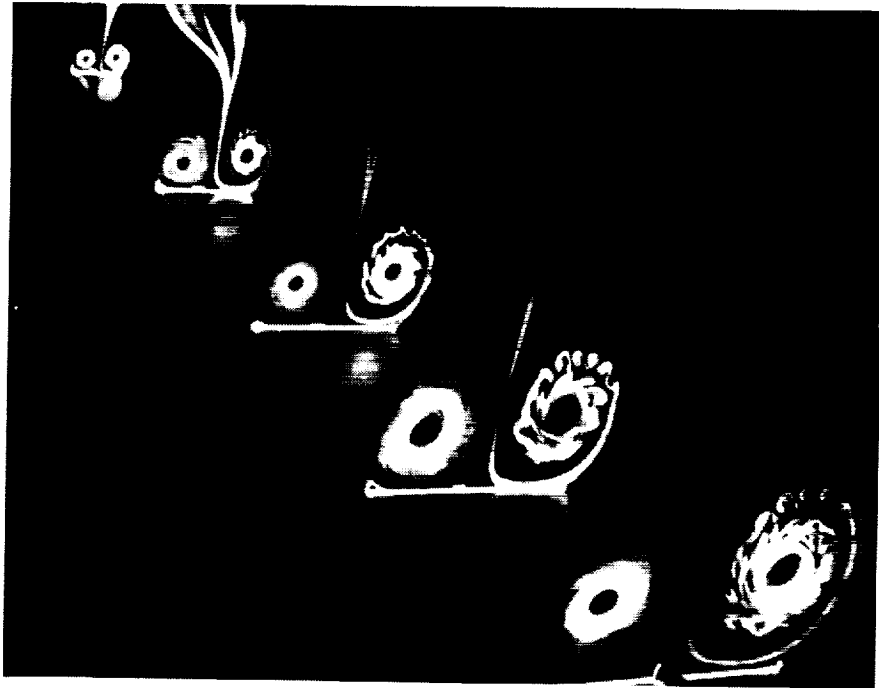


Figure A31. Lateral laser sheet cross sections.
Sweep = 85° , Alpha = 30° , U = 3.0 m/s.

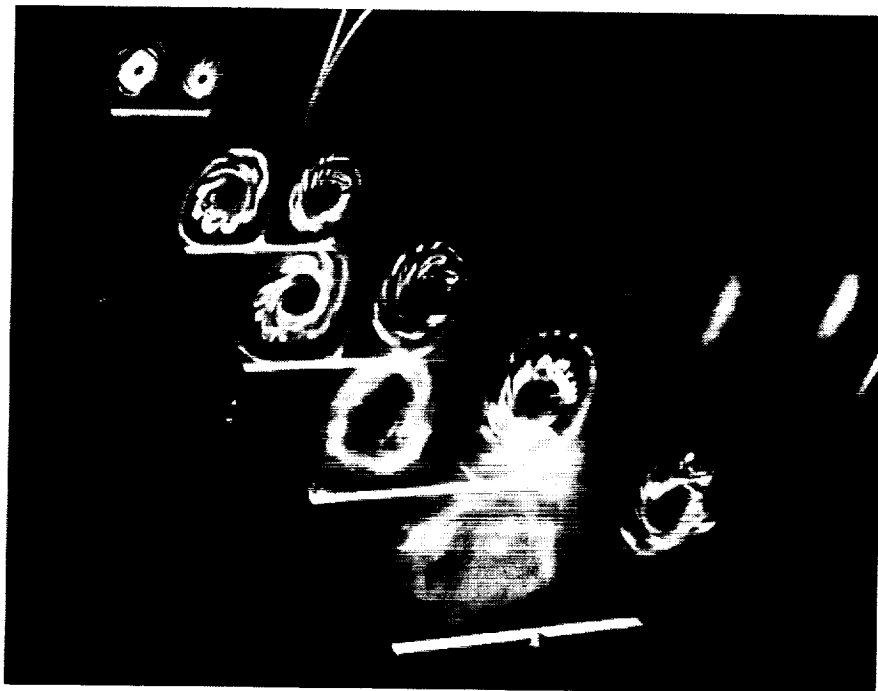


Figure A32. Lateral laser sheet cross sections.
Sweep = 85° , Alpha = 40° , U = 3.0 m/s.

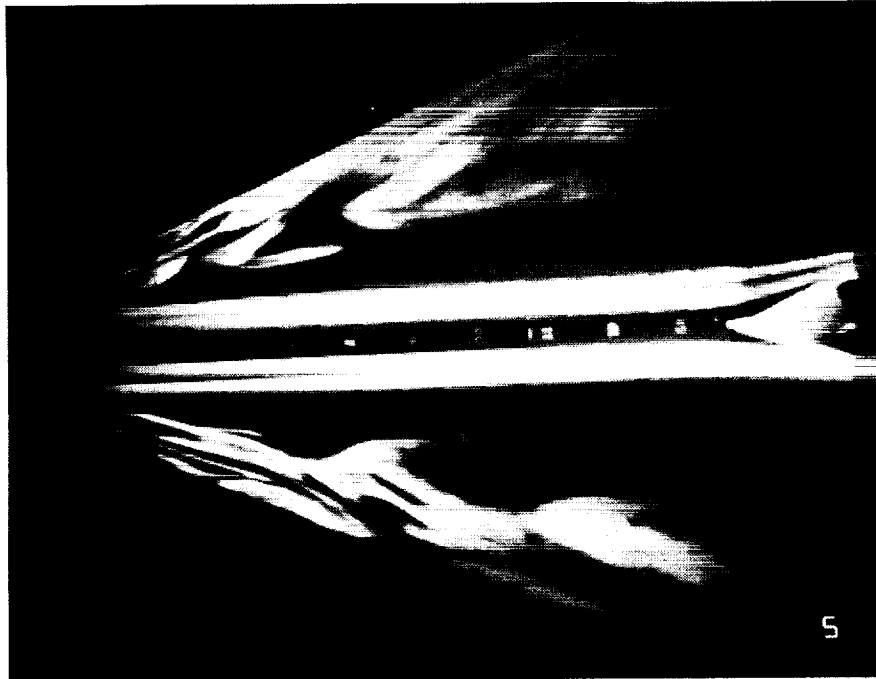


Figure A33. Longitudinal laser sheet cross section.
Sweep = 70° , Alpha = 10° , U = 3.0 m/s.



Figure A34. Longitudinal laser sheet cross section.
Sweep = 70° , Alpha = 20° , U = 3.0 m/s.



Figure A35. Longitudinal laser sheet cross section.
Sweep = 70° , Alpha = 30° , U = 3.0 m/s.

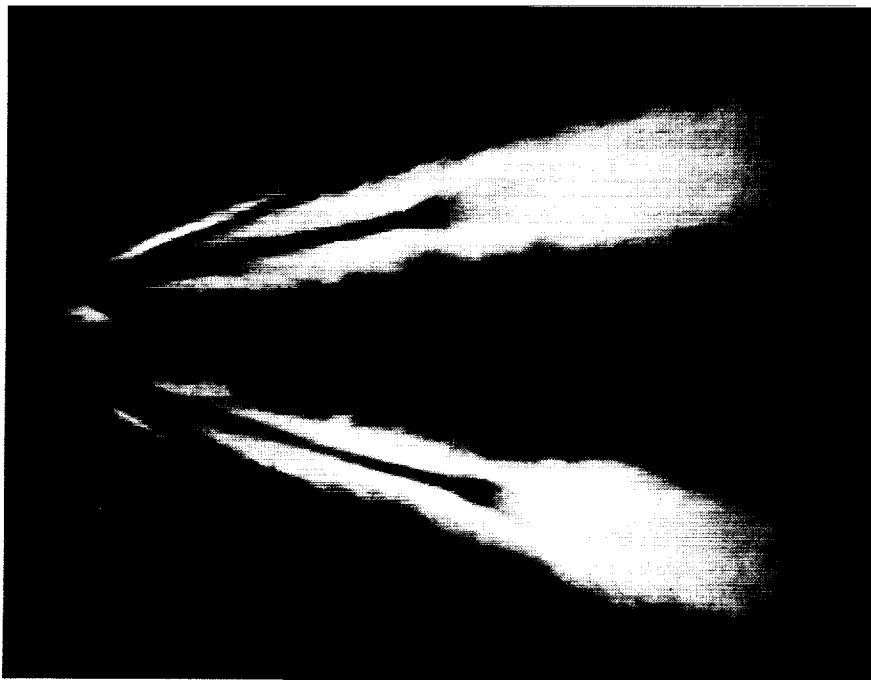


Figure A36. Longitudinal laser sheet cross section.
Sweep = 70° , Alpha = 40° , U = 3.0 m/s.

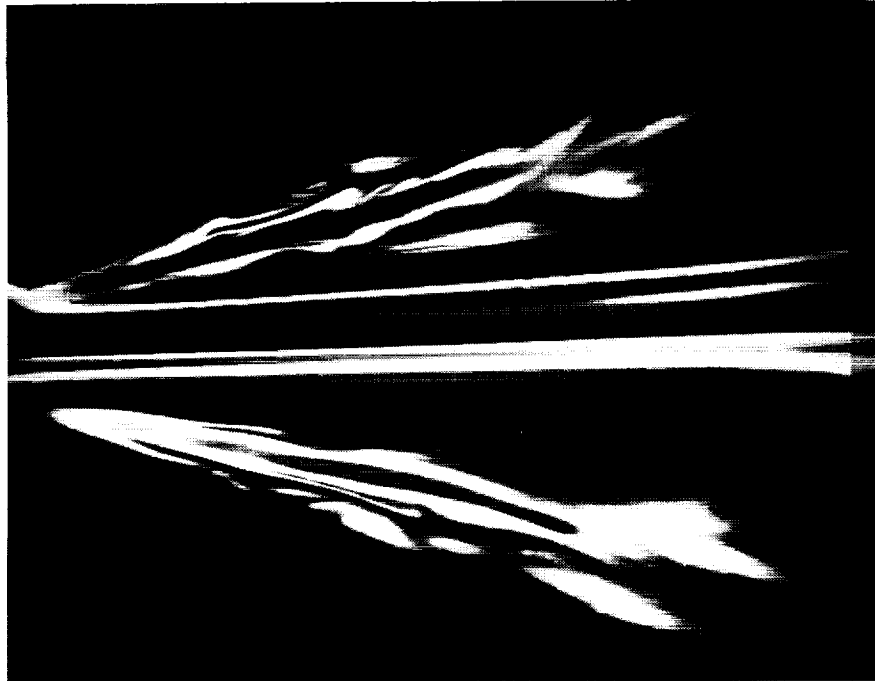


Figure A37. Longitudinal laser sheet cross section.
Sweep = 75° , Alpha = 10° , U = 3.0 m/s.

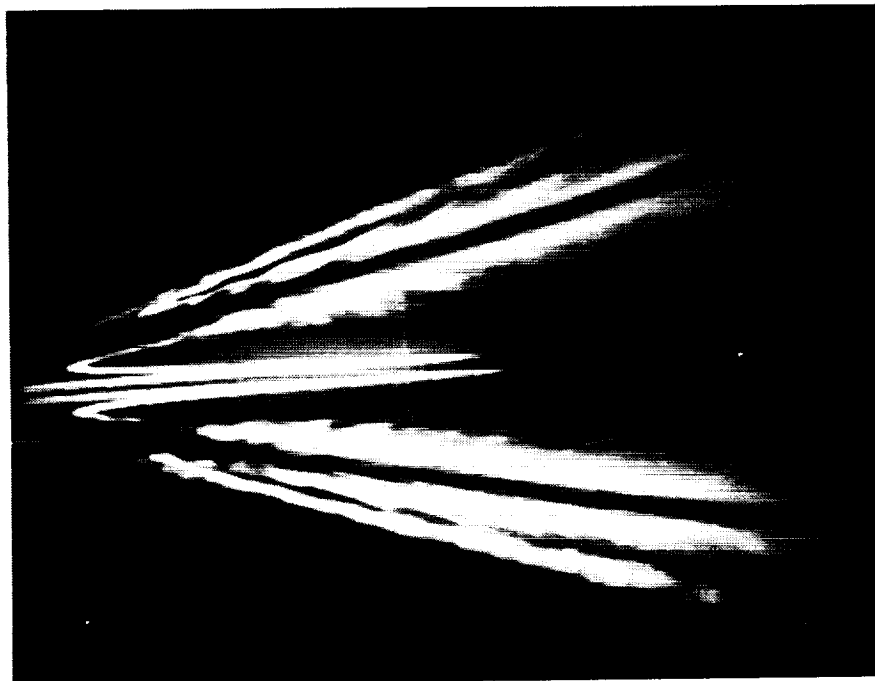


Figure A38. Longitudinal laser sheet cross section.
Sweep = 75° , Alpha = 20° , U = 3.0 m/s.



Figure A39. Longitudinal laser sheet cross section.
Sweep = 75° , Alpha = 30° , U = 3.0 m/s.



Figure A40. Longitudinal laser sheet cross section.
Sweep = 75° , Alpha = 40° , U = 3.0 m/s.

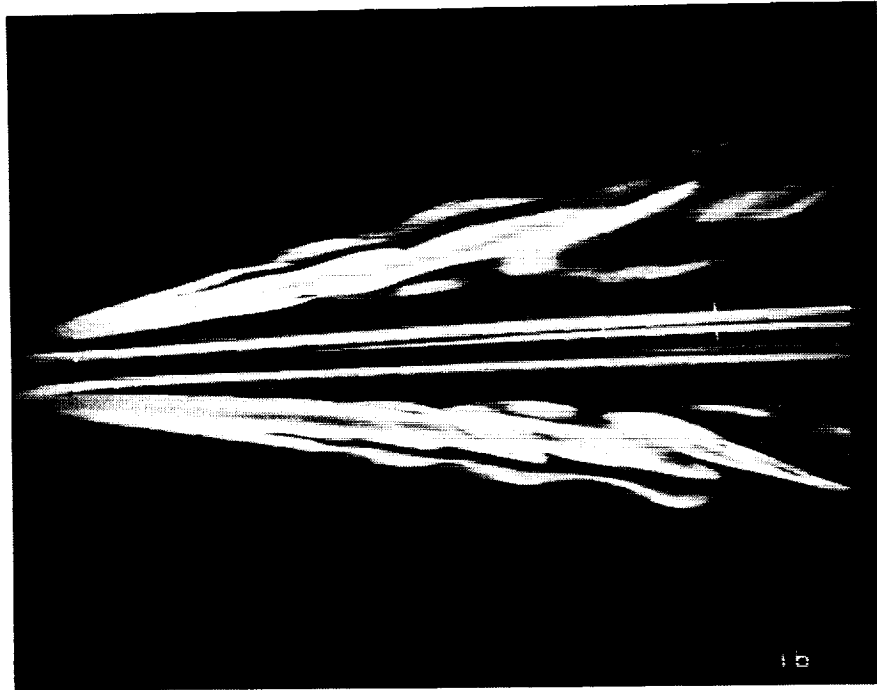


Figure A41. Longitudinal laser sheet cross section.
Sweep = 80° , Alpha = 10° , U = 3.0 m/s.

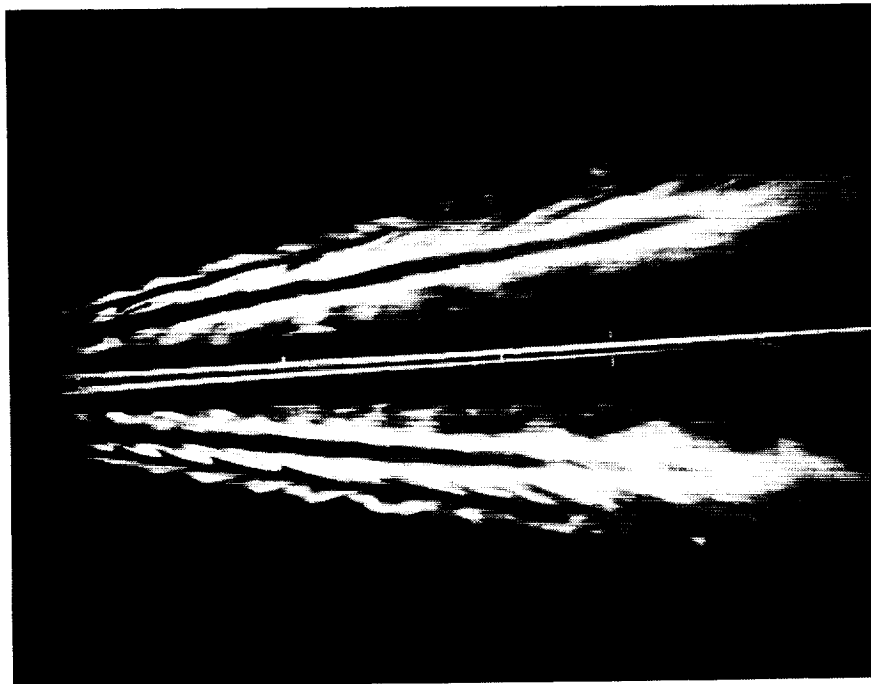


Figure A42. Longitudinal laser sheet cross section.
Sweep = 80° , Alpha = 20° , U = 3.0 m/s.

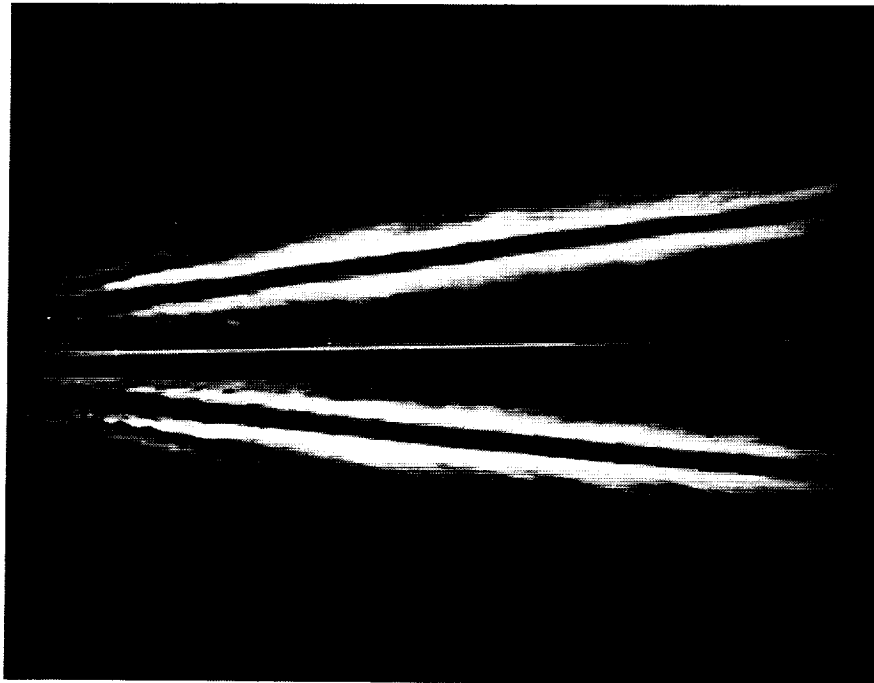


Figure A43. Longitudinal laser sheet cross section.
Sweep = 80° , Alpha = 30° , U = 3.0 m/s.



Figure A44. Longitudinal laser sheet cross section.
Sweep = 80° , Alpha = 40° , U = 3.0 m/s.

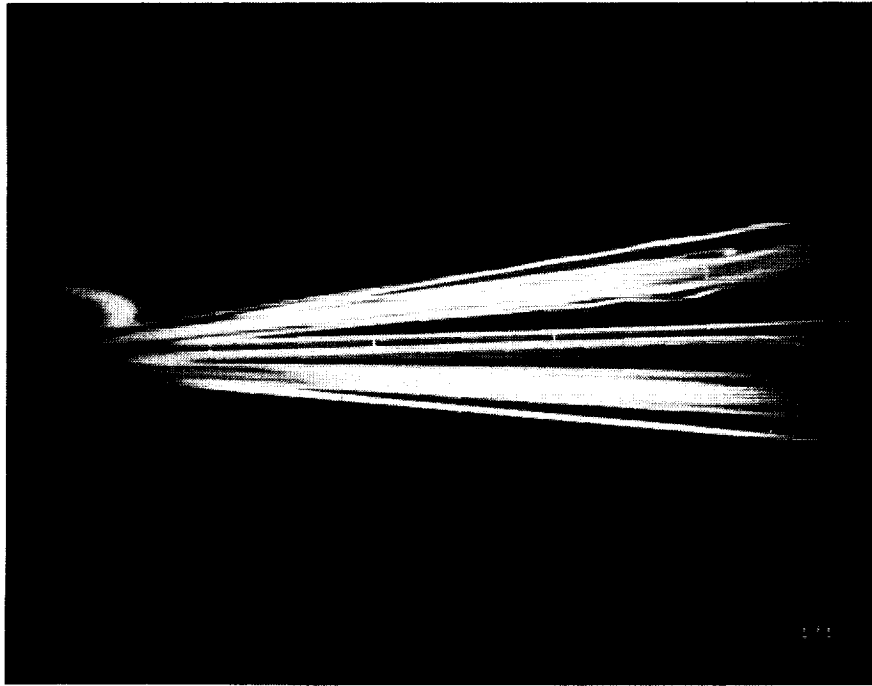


Figure A45. Longitudinal laser sheet cross section.
Sweep = 85° , Alpha = 10° , U = 3.0 m/s.

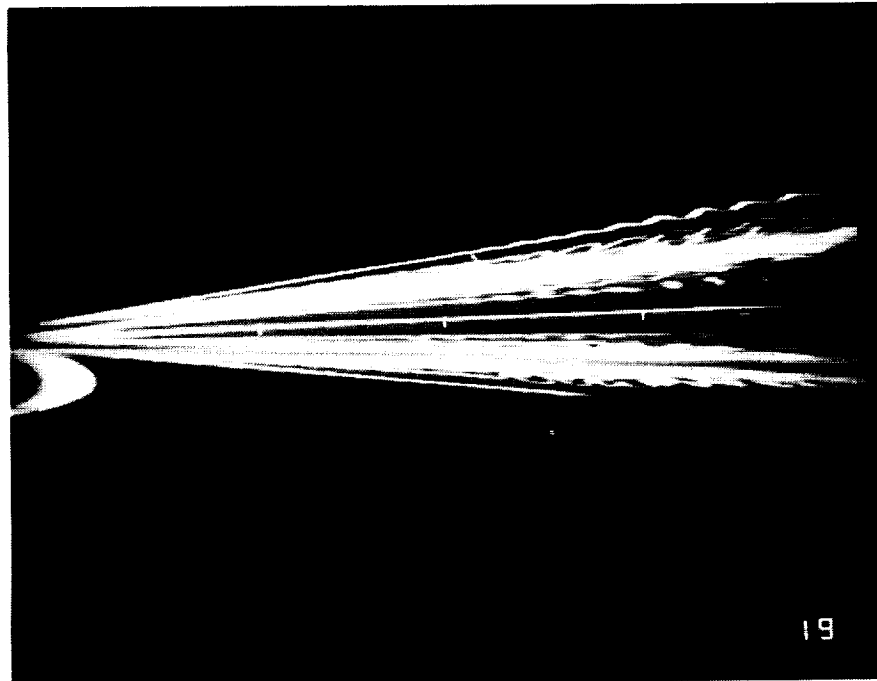


Figure A46. Longitudinal laser sheet cross section.
Sweep = 85° , Alpha = 20° , U = 3.0 m/s.



Figure A47. Longitudinal laser sheet cross section.
Sweep = 85° , Alpha = 30° , U = 3.0 m/s.

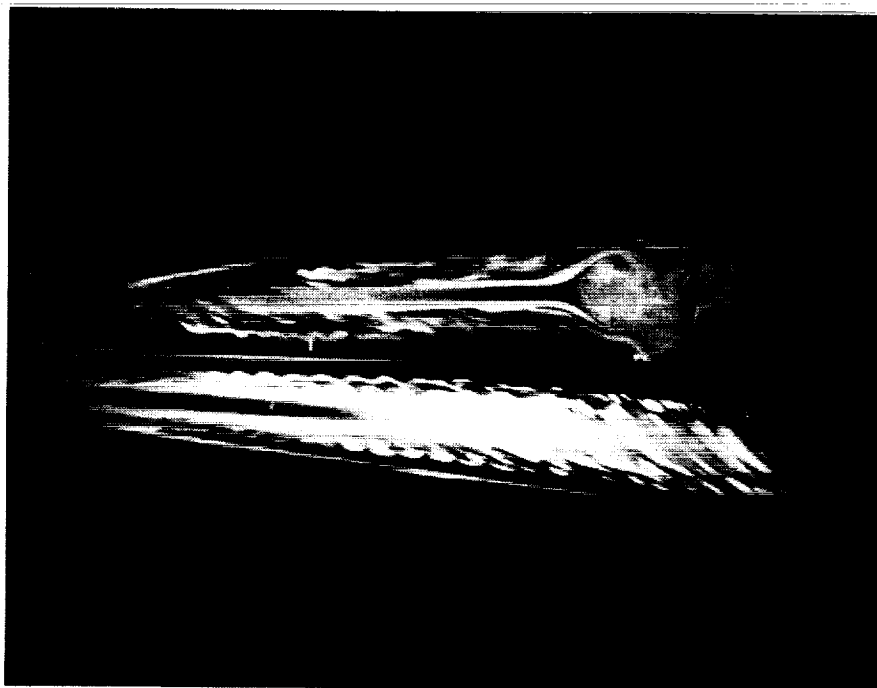


Figure A48. Longitudinal laser sheet cross section.
Sweep = 85° , Alpha = 40° , U = 3.0 m/s.

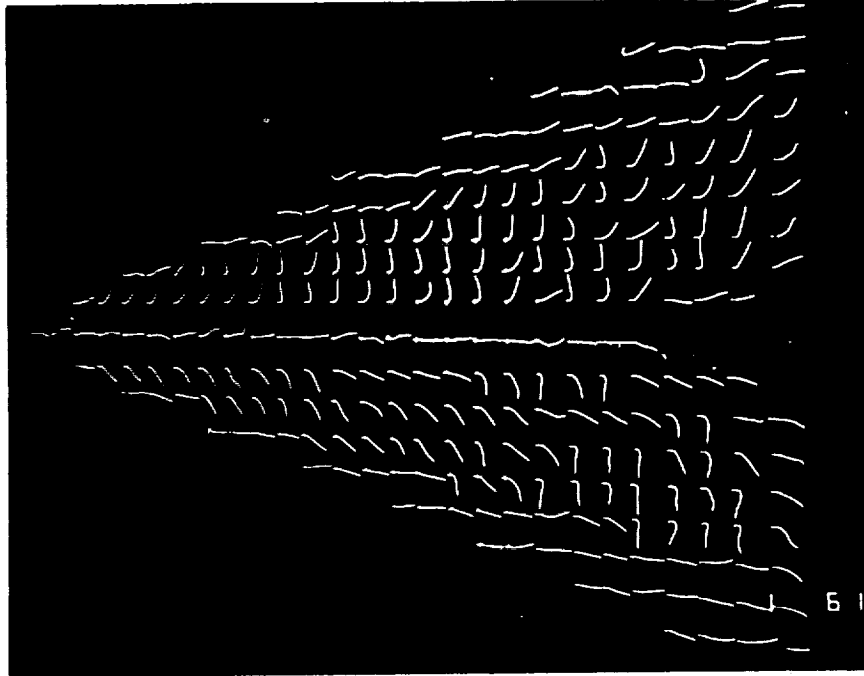


Figure A49. Fluorescent mini-tufts. Sweep = 70° ,
Alpha = 10° , U = 15.2 m/s.

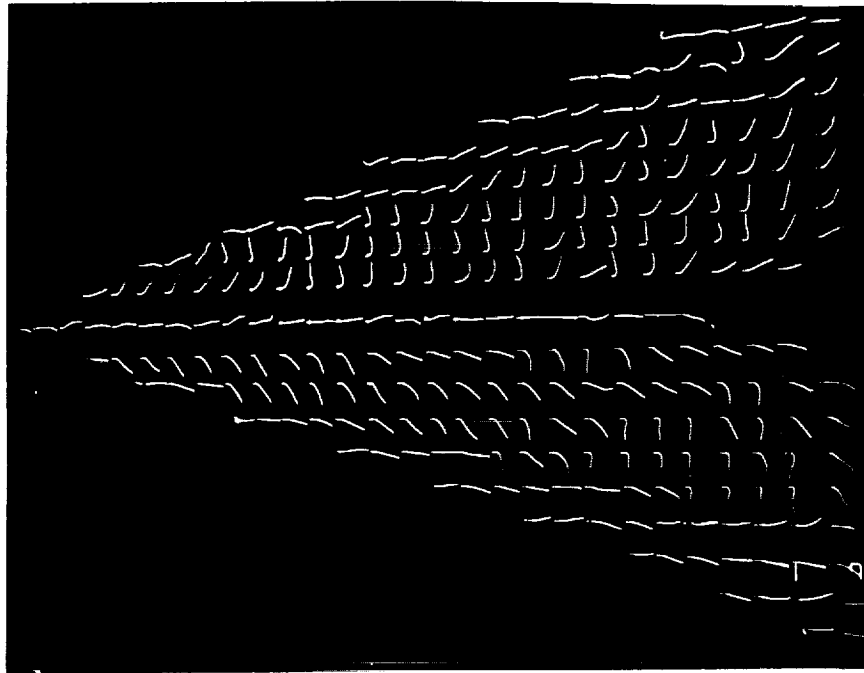


Figure A50. Fluorescent mini-tufts. Sweep = 70° ,
Alpha = 20° , U = 15.2 m/s.

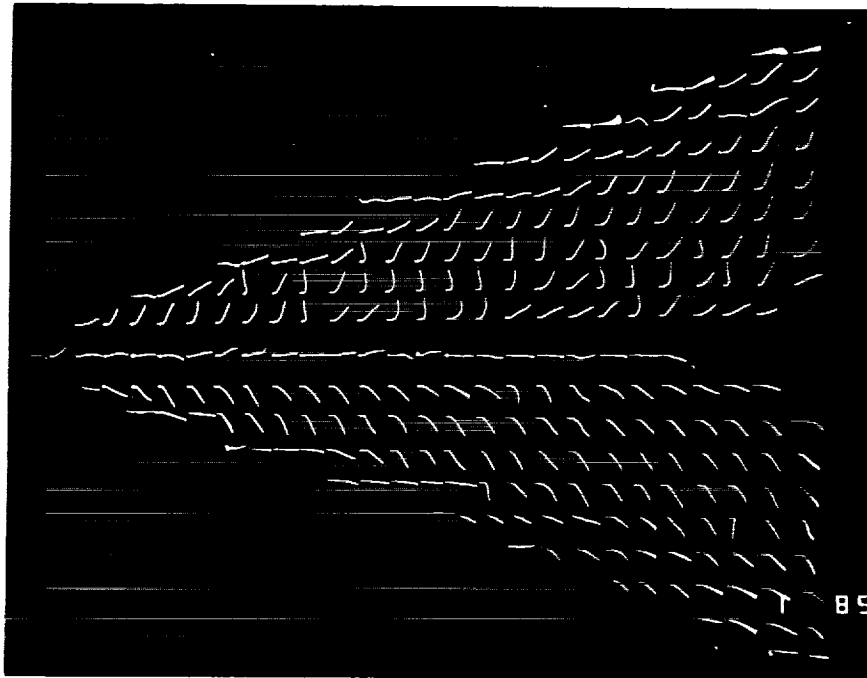


Figure A51. Fluorescent mini-tufts. Sweep = 70,
Alpha = 30°, U = 15.2 m/s.

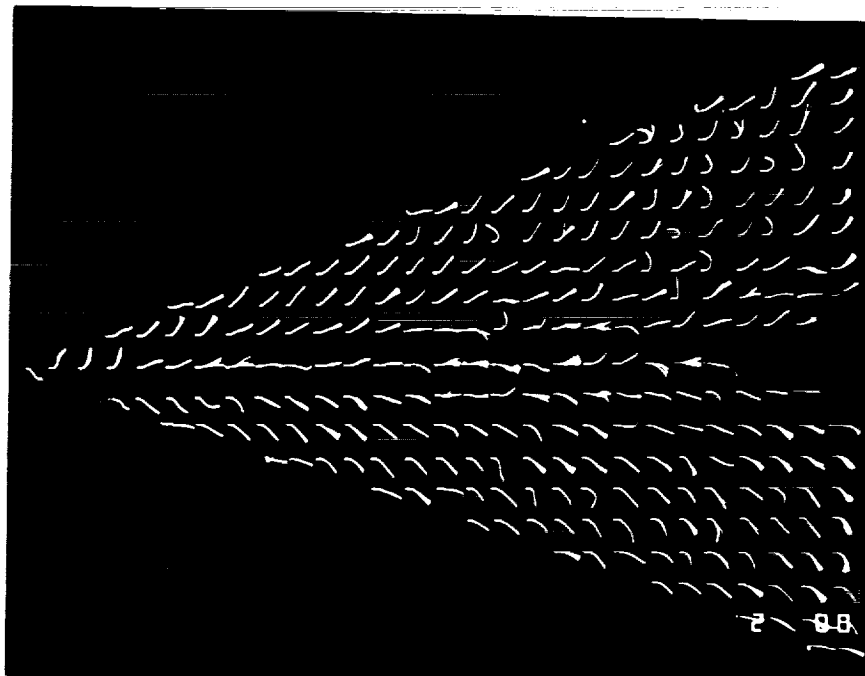


Figure A52. Fluorescent mini-tufts. Sweep = 70,
Alpha = 40°, U = 15.2 m/s.

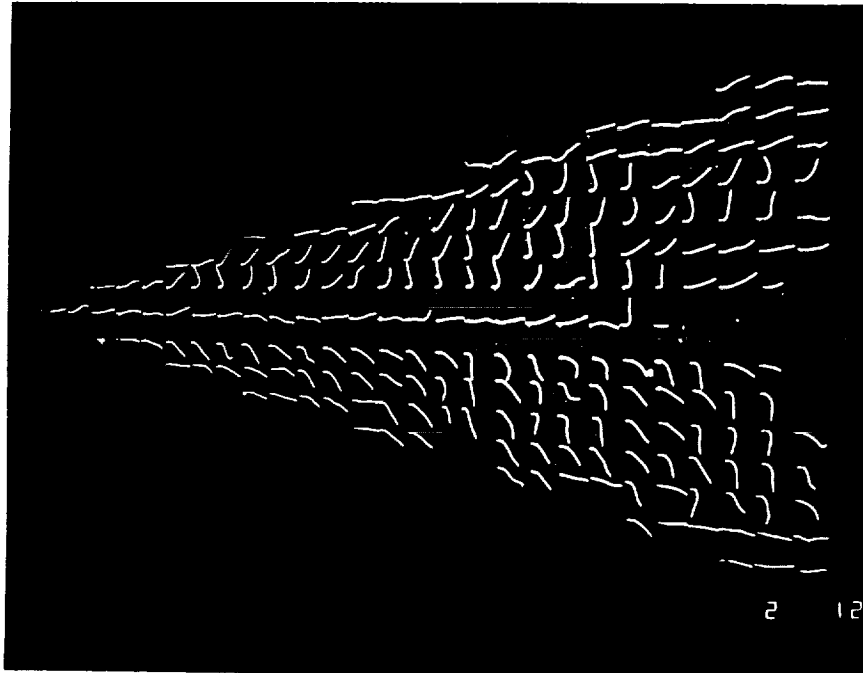


Figure A53. Fluorescent mini-tufts. Sweep = 75° ,
Alpha = 10° , $U = 15.2$ m/s.

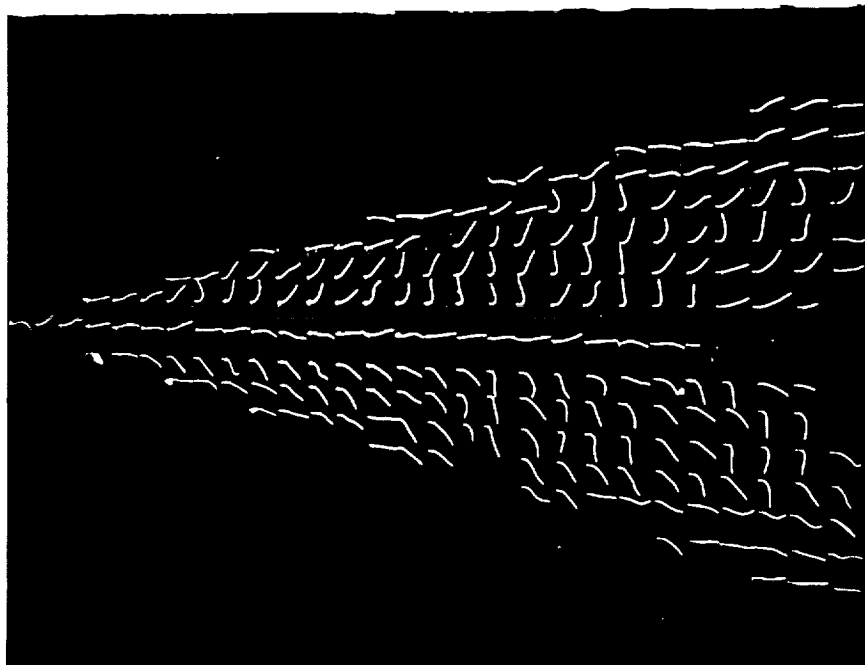


Figure A54. Fluorescent mini-tufts. Sweep = 75° ,
Alpha = 20° , $U = 15.2$ m/s.

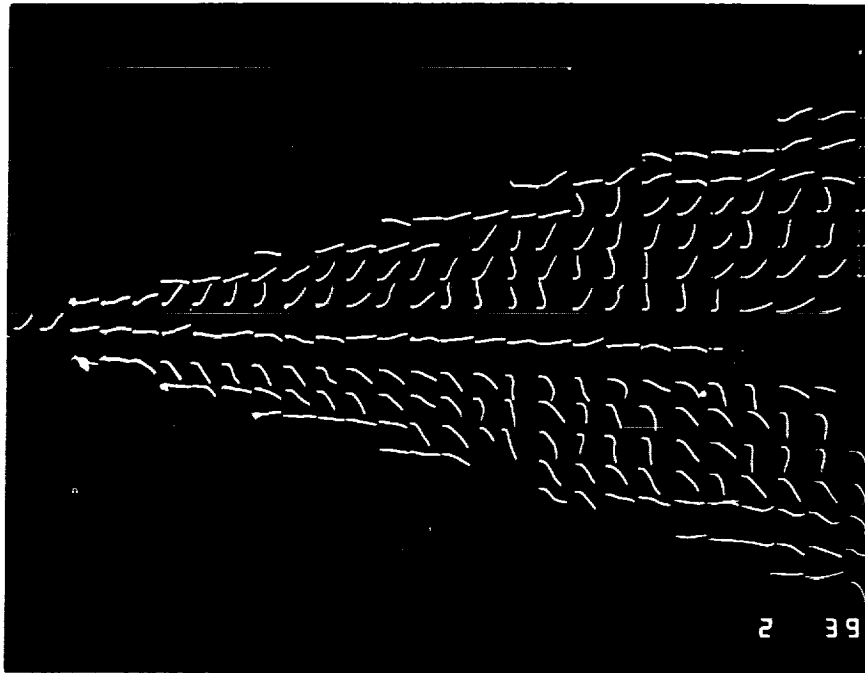


Figure A55. Fluorescent mini-tufts. Sweep = 75° ,
Alpha = 30° , $U = 15.2$ m/s.

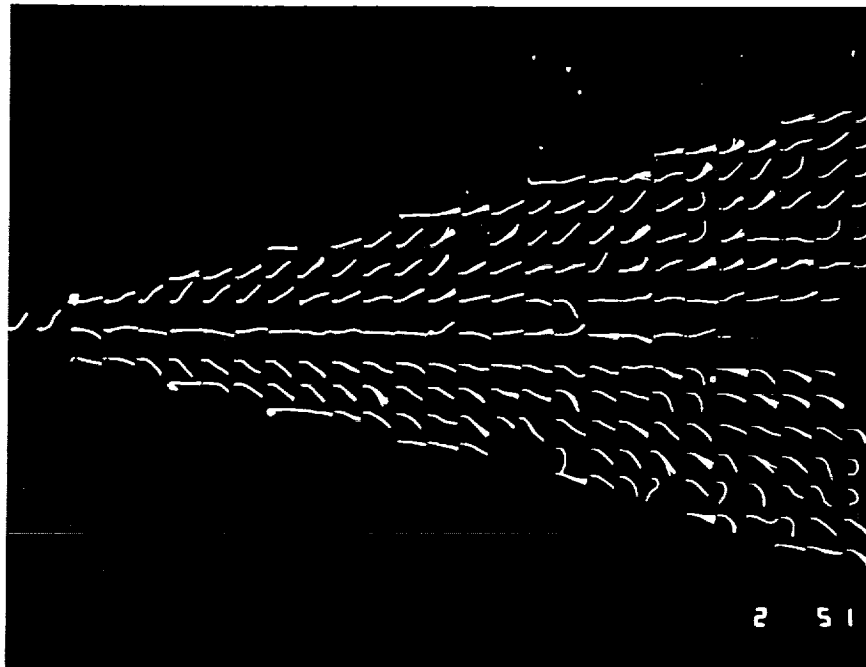


Figure A56. Fluorescent mini-tufts. Sweep = 75° ,
Alpha = 40° , $U = 15.2$ m/s.

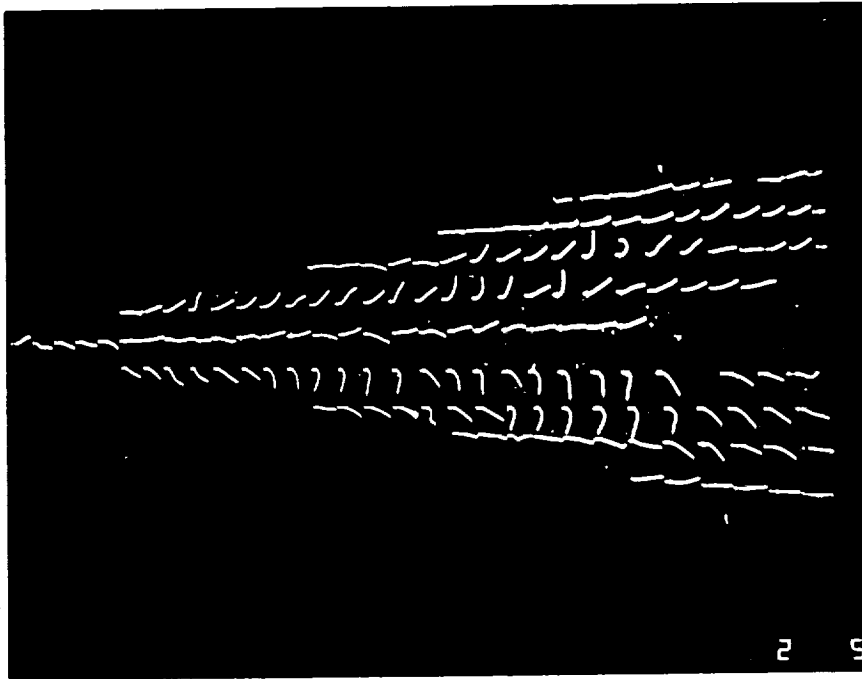


Figure A57. Fluorescent mini-tufts. Sweep = 80° ,
Alpha = 10° , U = 15.2 m/s.

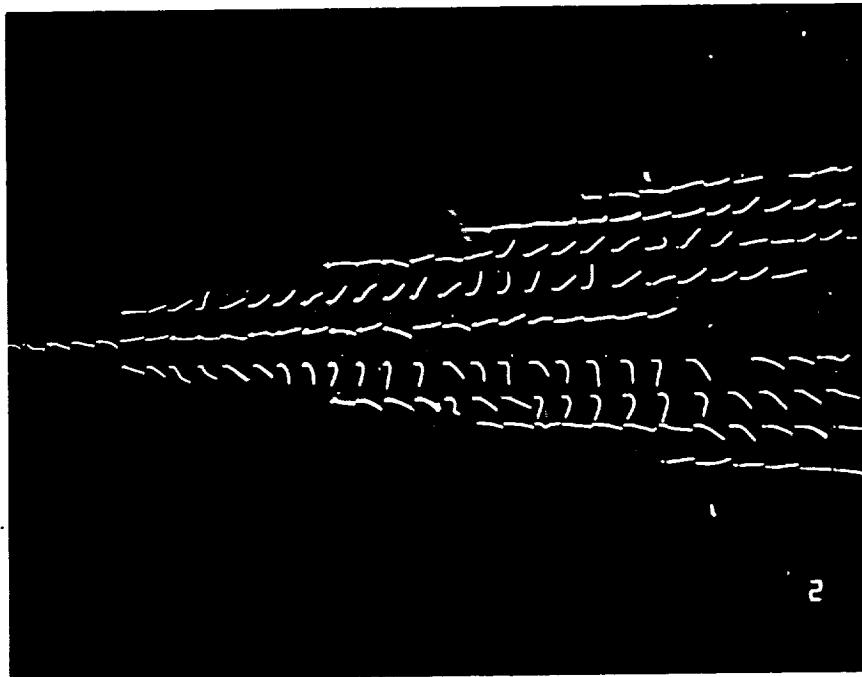


Figure A58. Fluorescent mini-tufts. Sweep = 80° ,
Alpha = 20° , U = 15.2 m/s.

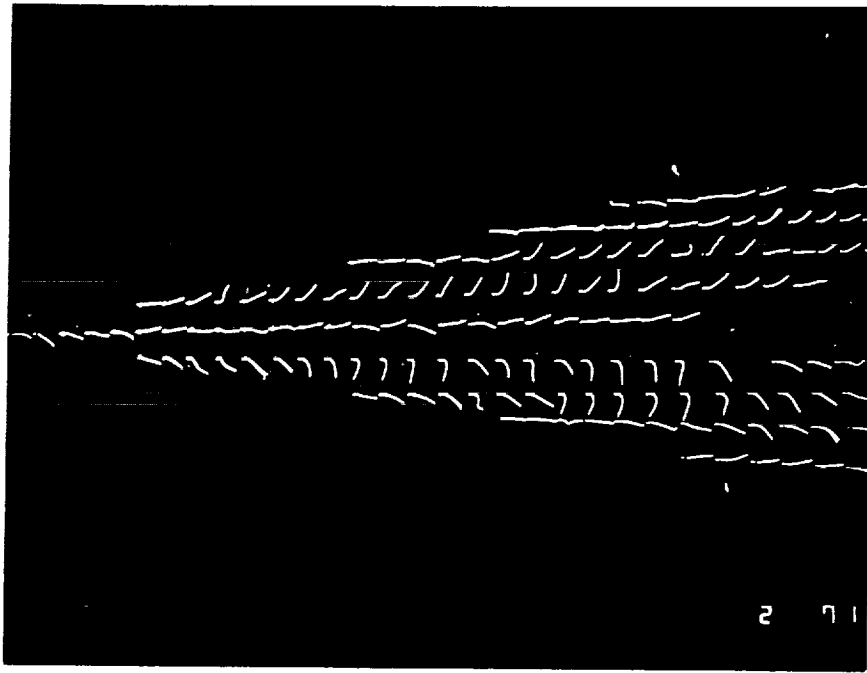


Figure A59. Fluorescent mini-tufts. Sweep = 80° ,
Alpha = 30° , U = 15.2 m/s.

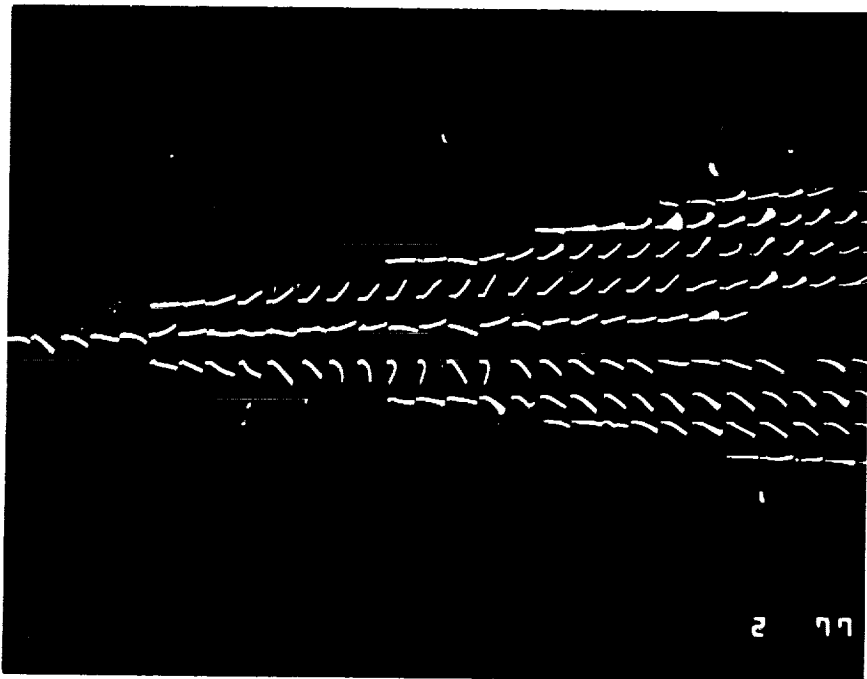


Figure A60. Fluorescent mini-tufts. Sweep = 80° ,
Alpha = 40° , U = 15.2 m/s.

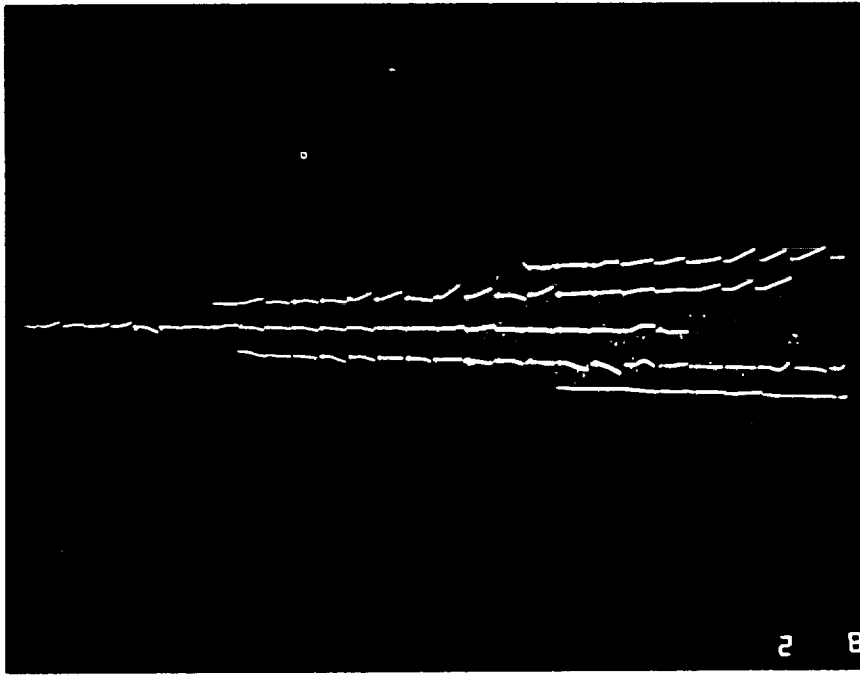


Figure A61. Fluorescent mini-tufts. Sweep = 85° ,
Alpha = 10° , U = 15.2 m/s.

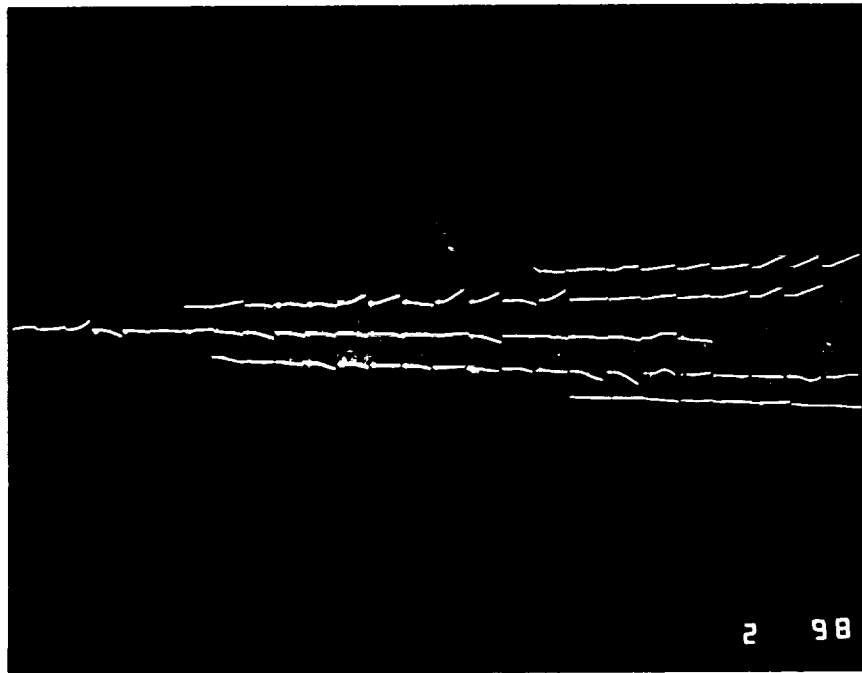


Figure A62. Fluorescent mini-tufts. Sweep = 85° ,
Alpha = 20° , U = 15.2 m/s.

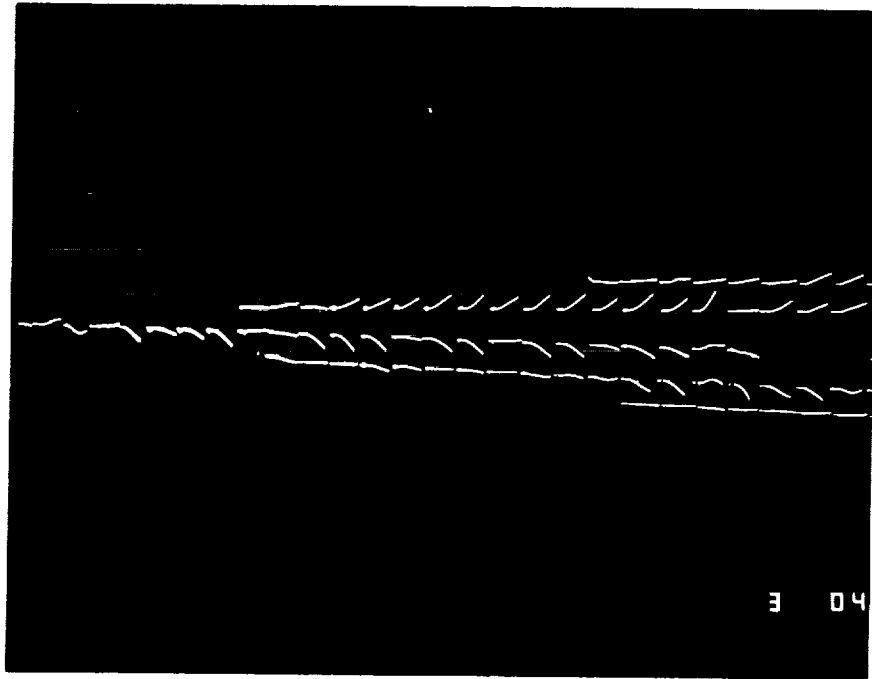


Figure A63. Fluorescent mini-tufts. Sweep = 85° ,
Alpha = 30° , U = 15.2 m/s.

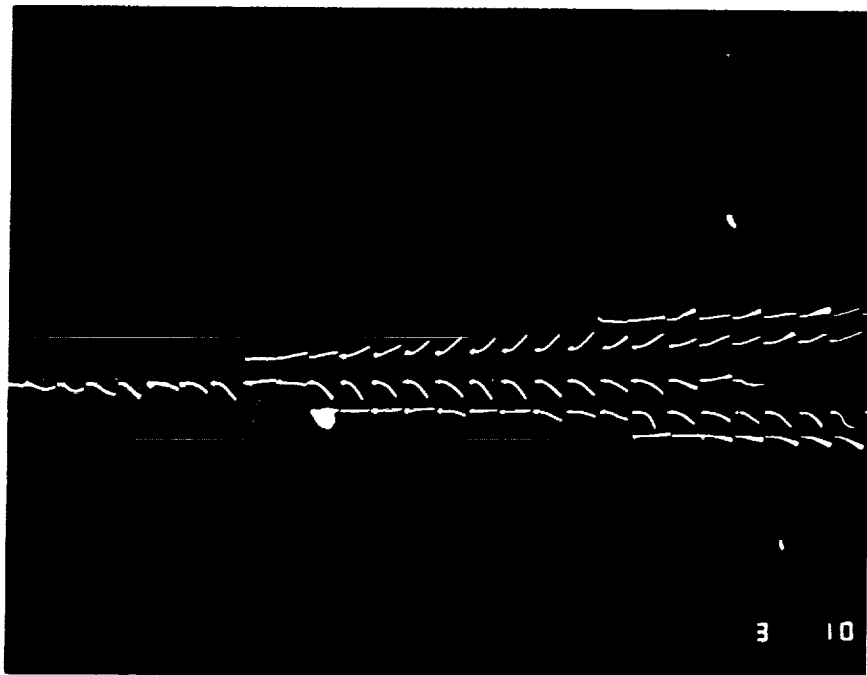


Figure A64. Fluorescent mini-tufts. Sweep = 85° ,
Alpha = 40° , U = 15.2 m/s.



Report Documentation Page

1. Report No. NASA CR-4320		2. Government Accession No.		3. Recipient's Catalog No.	
4. Title and Subtitle Visualization of Leading Edge Vortices on a Series of Flat Plate Delta Wings			5. Report Date April 1991		
			6. Performing Organization Code		
7. Author(s) Francis M. Payne, T. Terry Ng, and Robert C. Nelson			8. Performing Organization Report No. A-90094		
			10. Work Unit No. 505-61-71		
9. Performing Organization Name and Address Department of Aerospace and Mechanical Engineering University of Notre Dame Notre Dame, IN 56556			11. Contract or Grant No. NAG2-258		
			13. Type of Report and Period Covered Contractor Report		
12. Sponsoring Agency Name and Address National Aeronautics and Space Administration Washington, DC 20546-0001			14. Sponsoring Agency Code		
			15. Supplementary Notes Point of Contact: Larry Erickson, Ames Research Center, MS 227-2, Moffett Field, CA 94035-1000 (415) 604-6217 or FTS 464-6217		
16. Abstract This report presents a summary of flow visualization data obtained as part of NASA Grant NAG2-258. During the course of this study, many still and high speed motion pictures were taken of the leading edge vortices on a series of flat plate delta wings at angle of attack. The purpose of this report is to present a systematic collection of photographs showing the state of the vortices as a function of angle of attack for the four models tested.					
17. Key Words (Suggested by Author(s)) Flow visualization Vortex flows Vortex breakdown Leading edge vortices			18. Distribution Statement Unclassified-Unlimited Subject Category - 02		
19. Security Classif. (of this report) Unclassified		20. Security Classif. (of this page) Unclassified		21. No. of Pages 84	22. Price A05

